Electrostatics Control Nanoparticle Interactions with Model and Native Cell Walls of Plants and Algae

Journal:	*Environmental Science & Technology*
Manuscript ID	es-2023-056865.R1
Manuscript Type:	Article
Date Submitted by the Author:	n/a
Complete List of Authors:	Jeon, Su-Ji; University of California Riverside, Botany and Plant Sciences Hu, Peiguang; University of California Riverside, Botany and Plant Sciences Kim, Kyoungtea; University of Wisconsin Madison, Molecular and Environmental Toxicology Anastasia, Caroline; Johns Hopkins University Kim, Hye-In; University of California Riverside Castillo, Christopher; University of California Riverside, Botany and Plant Sciences Ahern, Colleen; University of California Riverside, Botany and Plant Sciences Pedersen, Joel; Johns Hopkins University, Department of Environmental Health and Engineering Fairbrother, D. Howard; Johns Hopkins University, Chemistry Giraldo, Juan Pablo; University of California Riverside, Botany and Plant Sciences

Electrostatics control nanoparticle interactions with model and native cell walls of plants and algae

Su-Ji Jeon[1#], Peiguang Hu[1#], Kyoungtea Kim[2#], Caroline M. Anastasia[3#], Hye-In Kim[1], Christopher Castillo[1], Colleen Ahern[1], Joel A. Pedersen[2,4], Howard Fairbrother[3], Juan Pablo Giraldo[1]*

[1]Department of Botany and Plant Sciences, University of California, Riverside, California, 92521, United States

[2]Molecular and Environmental Toxicology, University of Wisconsin—Madison, Madison, Wisconsin 53706, United States

[3]Department of Chemistry, Johns Hopkins University, Baltimore, Maryland 21218, United States

[4]Department of Environmental Health and Engineering, Johns Hopkins University, Baltimore, Maryland 21218, United States

[*]Corresponding Author: juanpablo.giraldo@ucr.edu

ABSTRACT

A mechanistic understanding of nanomaterial interactions with plant and algae cell walls limits the advancement of nanotechnology-based tools for sustainable agriculture. We systematically investigated the influence of nanoparticle charge on the interactions with model cell wall surfaces built with cellulose or pectin and performed comparative analysis with native cell walls of *Arabidopsis* plants and green algae (*Choleochaete*). The high affinity of positively charged carbon dots (CDs) (46.0±3.3 mV, 4.3±1.5 nm) to both model and native cell walls was dominated by the strong ionic bonding between the surface amine groups of CDs and the carboxyl groups of pectin. In contrast, these CDs formed weaker hydrogen bonding with hydroxyl groups of cellulose model surfaces. The CDs of similar size with negative (-46.2±1.1 mV, 6.6±3.8 nm) or neutral (-8.6±1.3 mV, 4.3±1.9 nm) zeta potential exhibited negligible interactions with cell walls. Real-time monitoring of CD interactions with model pectin cell walls indicated higher absorption efficiency (0.03±0.001) and acoustic mass density (313.3±63.3 ng cm^{-2}) for positively charged CDs than negative and neutral counterparts (p<0.001 and p<0.01, respectively). The surface charge density of positively charged CDs significantly enhanced these electrostatic interactions with cell walls, pointing to approaches to control nanoparticle binding to plant biosurfaces. Ca^{2+} induced cross-linking of pectin affected the initial absorption efficiency of positively charged CD on cell wall surfaces (~3.75 times lower) but not the accumulation of the nanoparticles to cell wall surfaces. This study developed model biosurfaces for elucidating fundamental interactions of nanomaterials with cell walls, a main barrier for nanomaterial translocation in plants and algae in the environment, and for the advancement of nano-enabled agriculture with reduced environmental impact.

KEYWORDS: Carbon nanomaterials, plant membranes, pectin, cellulose, environmental nanotechnology, nano-enabled agriculture.

SYNOPSIS: This study elucidates mechanisms of nanomaterial interactions with plant and algae cell walls, an outer cell layer present in these key photosynthetic organisms that support life on earth.

INTRODUCTION

Food production needs to increase by about 60% to support the predicted global population growth to almost 10 billion by 2050.[1–3] However, the growth rates of global agricultural yields are far behind what is required to achieve this food production goal.[4] This is an increasingly challenging task as global climate change induces more frequent and severe environmental stresses.[5] Various nanotechnology-based strategies have been proposed to increase crop yields including targeted plasmid DNA delivery and up to 80% transformation efficiency for plant genetic modifications,[6–10] improved pesticide and nutrient delivery efficiency by 20-30%,[4,11–14] and sensors to for early detection of the onset of crop stress.[11,15–17] The emerging use of engineered nanomaterials as tools for agriculture has also sparked interest in understanding their impact on plant function and the environment.[2,18–21]

All photosynthetic multicellular Eukaryotes on earth, including plants and algae, have cells that are surrounded by a cell wall that plays a key role controlling environmental interactions with individual cells and organisms.[22] The cell wall is a crucial biosurface that has been identified as one of the main barriers encountered by nanomaterials in terrestrial plants[23] and algae in aquatic ecosystems.[24,25] A lack of mechanistic understanding of nanoparticle-plant cell wall interactions limits our ability to develop efficient and sustainable nanomaterials for agriculture applications with low environmental impact. For example, the plant cell wall is a main barrier for nanomaterial mediated delivery of DNA for plant genetic modification,[7,26,27] and delivery of nutrients and pesticides for crop growth and yield improvement.[4,20,26,28] Previous studies reported that nanoparticle size and charge influence the uptake of nanomaterials through plant cell and organelle lipid membranes,[29,30] and mediate the translocation and

distribution of nanoparticles in plants *in vivo*.[31,32] A zeta potential with a magnitude above 20 or 30 mV, whether positive or negative, has been reported to facilitate nanomaterials penetration of isolated protoplast membranes lacking cell walls or chloroplast lipid membranes, respectively.[29,30] The delivery efficiency of nanoparticles into plant cells and organelles *in vivo* was reported to be affected by the size and charge, and hydrophobicity of nanoparticles.[31–36] Positively charged and hydrophilic nanoparticles preferentially localize inside leaf mesophyll or cortex root cells and organelles;[31,37] whereas negatively charged nanoparticles have been mainly observed to translocate in vascular tissues including stomata guard cells, xylem and the phloem.[31,38] Hydrophobic coatings enhance the translocation across leaf cell walls of nanoparticles up to 50 nm in size.[32] In these studies, the plant cell wall was identified as a main barrier for nanoparticle uptake into plant cells but the mechanisms of these interactions were not elucidated. Studies in bacteria and green algae have reported opposite interactions and effects of nanoparticle charge on their cell walls while the underlying physical and chemical mechanisms of these interactions remains unknown.[24,39] Quantitative analysis of the interactions between nanoparticles and biosurfaces have largely focused on attachment to the organism lipid membranes[40–45] without addressing the outermost cell wall biosurface that is characteristic of major organism taxa including plants and algae. The mechanisms of interactions with bacteria cell walls formed by lipopolysaccharides and peptidoglycans[46] cannot be extrapolated to those of cell walls of plants and algae having a distinct composition of cellulose, pectin, and other non-lipid based molecules. Currently, we lack studies providing a mechanistic understanding of how nanomaterial properties influence their interactions with cell walls of photosynthetic organisms that support life on earth.

The primary cell wall is mainly formed by cellulose microfibrils interwoven in a network of pectic polysaccharides that creates a biosurface varying between ~100 and >1,000 nm in thickness.[47] Although cell wall pore diameters measured by electron microscopy are mainly below 10 nm with a

maximum of 20 nm, the pore size of cell walls has been reported to allow the translocation of nanoparticles up to 50 nm.[23] The main components of the plant cell walls are cellulose, non-cellulosic and pectic polysaccharides, proteins, phenolic compounds, and water, among which polysaccharides like cellulose and pectin are the major components (> 90%).[48,49] Cellulose is a homopolymer of glucose joined by β-1,4 linkages with a relatively neutral charge,[50] acting as a water-insoluble carbohydrate that maintains the structural integrity of the plant cell walls.[48] Pectin is a very complex macromolecule defined as a negatively charged hetero-polysaccharide with the predominant component of galacturonic acid residues, where part of the acid groups is esterified to varying degrees.[48,51,52] The weak disassociation of the acidic groups in pectin confers the plant cell walls a net negative charge.[53] This allows the plant cell walls to bind cations such as calcium in negatively charged sites and behave as ion exchange polymers facilitating cation translocation across plant cell walls.[54] The chemical interactions between amine functional groups of positively charged nanoparticles and carboxyl and hydroxyl groups of pectin and cellulose, respectively, have been proposed to play a key role in determining nanoparticle translocation and distribution in plant cells.[31 34,35] However, the lack of model cell wall surfaces has been a limitation to demonstrate, understand and quantify the interaction between functional groups on nanoparticles and components of the cell wall surfaces.

Herein, we studied the interactions between model and native plant cell walls with carbon dots (CDs) of different surface charge that were coated with polyethylenimine (PEI-CD), carboxylated polyethylenimine (CP-CD), and polyvinylpyrrolidone (PVP-CD) (Figure 1). We also examined the effect of nanoparticle surface charge density on the interactions between cell walls and nanoparticles. The CDs were chosen as model nanoparticles due to their agricultural applications and environmental significance, and their optical properties allowing imaging by confocal fluorescence microscopy. Recent

studies have reported that CDs enhance plant growth,[55–58] resistance to disease[59] and can be used as fertilizers.[57,58] CD fluorescence properties also allow environmental monitoring and detection of pesticides.[60–62] The CD small size below the reported cell wall exclusion limit (<50 nm)[23] and their water solubility[63] allowed us to focus on elucidating the role of nanoparticle charge without other confounding properties (e.g. size and hydrophobicity). We elucidated the chemical interactions of plant cell wall model surfaces with CDs using multiple analytical and quantitative tools including Fourier-transform infrared spectroscopy (FTIR), X-ray photoelectron spectroscopy (XPS), and real-time quartz crystal microbalance with dissipation monitoring (QCM-D) measurements. The results acquired with model surfaces were validated with interactions between CDs and native biosurfaces including cell walls isolated from *Arabidopsis* plants and cell walls of *Coleochaete*, a green algae closely related to terrestrial plants with similar cell wall composition.[64] A mechanistic understanding of nanomaterial-cell wall interactions based on model biosurfaces can advance the rational design of nanomaterials with controlled delivery in plants for a more sustainable nano-enabled agriculture.

MATERIALS AND METHODS

Model cell wall interactions with CDs. PEI-CD, CP-CD, and PVP-CD were diluted in DI water at a concentration of 10 μg/mL. The cellulose or pectin model surfaces mounted on glass slides were submerged horizontally in the CD suspensions for 10 min to interact with CDs, followed by immersion in DI water three times for 30 s each time to remove any unbound CDs. ATR-FTIR was performed with a Nicolet 6700 FTIR spectrometer in pectin and cellulose model cell walls on glass substrates before and after CD exposure. X-ray photoelectron spectroscopy was performed using a Kratos AXIS ULTRA DLD XPS system with pectin and cellulose model cell walls on glass substrates before and after CD treatments.

Confocal microscopy imaging. Cell wall model surfaces, isolated *Arabidopsis* plant cell walls, and *Coleochaete* green algae were imaged in an inverted Zeiss 880 confocal laser scanning microscope. Confocal microscopy imaging settings were as follows: 20 × dry objective; laser excitation 355 nm for CD fluorescence and 633 nm for chlorophyll fluorescence; z-stack section thickness = 2 μm; line average = 4; PMT 1 (CD channel), 370–500 nm, PMT 2 (chloroplast channel), 647–721 nm, and PMT 3 (bright field channel). At least three samples were used for confocal microscopy imaging. Cell wall model surfaces prepared on glass slides were directly used as microscopy samples. Isolated *Arabidopsis* plant cell walls and *Coleochaete* green algae microscopy samples were prepared as follows. Isolated *Arabidopsis* plant cell walls (1 mg/mL) with and without CD treatment were suspended in DI water as described above. Then a 5 μL solution was mounted on a microscope slide and covered with a coverslip. *Coleochaete* green algae in growth medium with and without CD treatment as described above were mounted on microscope slides within a Carolina observation gel chamber (~1 mm in thickness, ~8 mm in diameter) and sealed with a coverslip. Confocal imaging analyses of fluorescence intensity were normalized by the quantum yield of CDs for comparison.

AFM analysis of native and model cell wall surfaces. AFM imaging was performed using a Veeco Dimension 5000 SPM system (Veeco, USA). Native and model cell walls were prepared by drop-casting of cell wall suspension on a silicon wafer and washed out several times with DI water to adjust the amount of cell wall adsorbed on the substrate. DI water was completely dried out before AFM analysis.

XPS analysis of model and native cell wall surfaces. XPS spectra of the model pectin layer was collected using a Thermo Fisher Scientific K-Alpha X-ray Photoelectron Spectrometer with an Al K source (1486.6 eV). Survey scans were collected from 1350 eV to 0 eV with a pass energy of 100 eV and resolution of 1.00 eV/step. Detailed scans of the C(1s) region were acquired at 22 eV pass energy

with 0.2 eV/step resolution. Spectra were analyzed using CasaXPS software. For the native cell wall, XPS characterization was carried out by using a Kratos AXIS ULTRA^{DLD} XPS system equipped with an Al Ka X-ray source and a 165-mm mean radius electron energy hemispherical analyzer. XPS sample was prepared by sonication 3 mg of native cell walls in the 3 ml of TES buffer (pH 9) for 1 h. A 10 µl cell wall suspension was drop-casted on a Si wafer and washed with DI water and methanol. The XPS of the native cell walls was fitted in CasaXPS. XPS methods for determining functional groups in both model and native cell wall surfaces are reported in SI.

Quartz crystal microbalance with dissipation (QCM-D) monitoring. Adsorption of CD onto pectin model surfaces was determined by changes in frequency (Δf_n) and energy dissipation at the interface (ΔD_n) upon nanoparticle exposure. Quartz crystal microbalance with dissipation monitoring (QCM-D) was used to measure both Δf_n and ΔD_n, and measurements were conducted with a QSense Analyzer (Biolin Scientific). Energy dissipation is defined as:[65]

$$D = \frac{E_{dissipated}}{2\pi E_{stored}} \qquad \text{Eq. (1)}$$

where $E_{dissipated}$ is the energy dissipation per oscillation and E_{stored} is the energy stored in the system. We calculated energy dissipation of the experimental system with Qsense Dfind (ver. 1.2.2, Biolin Scientific, Gothenburg, Sweden). Because all data after rinse had ratio of $|\Delta D_n/(\Delta f_n/n)| > 4 \times 10^{-7}$ Hz^{-1}, we considered the bound CD on the pectin surface a rigid layer.[66] All measurement datasets fit Sauerbrey regime, thus we determined acoustic mass densities (Γ_{QCM-D}) at the interface from changes in frequency (Δf_n) using the Sauerbrey equation:[67]

$$\Gamma_{QCM\text{-}D} = -C\frac{\Delta f_n}{n} \quad \text{Eq. (2)}$$

where n is a harmonic number and C is the mass sensitivity constant for the experimental system, 18 ng·cm^{-2}·Hz^{-1}.[68] We report $\Gamma_{QCM\text{-}D}$ and ΔD_n of the 5th overtone (n = 5, *i.e.* ~25 MHz).

Adsorption efficiency. Adsorption efficiency of CDs onto pectin model surfaces (α) was determined by the ratio of experimental $d\Gamma_{QCM\text{-}D}/dt$ to theoretical $d\Gamma_{QCM\text{-}D}/dt$:[69]

$$\alpha = \frac{(d\Gamma_{QCM\text{-}D}/dt)_{experimental}}{(d\Gamma_{QCM\text{-}D}/dt)_{theoretical}} \quad \text{Eq. (3)}$$

where $d\Gamma_{QCM\text{-}D}/dt$ is average change in mass density per unit time for the first 100 s of pectin layer exposure to CDs. Experimental $d\Gamma_{QCM\text{-}D}/dt$ values were calculated by taking the first derivative of $\Gamma_{QCM\text{-}D}$ with respect to time over the first 100 s of detectable CD interaction with cell film. Theoretical $d\Gamma_{QCM\text{-}D}/dt$ values were calculated as:[70]

$$(d\Gamma_{QCM\text{-}D}/dt)_{theoretical} = k_a m_s e^{-(k_a m_s/\Gamma^*)t} \quad \text{Eq. (4)}$$

where m_s is the mass concentration of CDs in solution (g·m^{-3}), and Γ^* represents the maximum surface concentration of CDs (g·m^{-2}). The theoretical rate constant of adsorption, k_a, was defined as:[71]

$$k_a = D_c^{2/3} Q^{1/3} < n > \quad \text{Eq. (5)}$$

where D_c is the diffusion coefficient (m^2·s^{-1}) of the CDs used, Q is the flow rate of fluid (m^3·s^{-1}), and $<n>$ is an averaged geometrical constant, 4.44 ×10^3 m$^{-4/3}$, for the experimental system. Diffusion coefficients, D_c are defined by the Stokes-Einstein equation:[70]

$$D_c = \frac{k_B T}{6\pi\eta R} \quad \text{Eq. (6)}$$

where k_B is the Boltzmann constant ($kg \cdot m^2 \cdot s^{-2} \cdot K^{-1}$), T is the absolute temperature (K), η is the viscosity of the measurement solution ($kg \cdot m^{-1} \cdot s^{-1}$), and *R*, the hydrodynamic radius of the CD (m) determined by DLS.

Statistical analysis. Most statistical analyses were performed in either SPSS 20.0 software (IBM, New York, USA) or Prism (GraphPad, San Diego, USA). Zeta potentials, DLS, fluorescence intensity, mass changes, and QCM-D datasets were compared by one-way ANOVA followed by post hoc analyses using Tukey test.

RESULTS AND DISCUSSION

Carbon dot characterization. We designed and synthesized CDs coated in polyethylenimine (PEI-CD), carboxylated polyethylenimine (CP-CD), polyvinylpyrrolidone (PVP-CD) for studying the role of nanoparticle charge on the interactions with cell walls (Figure 2a). The nanoparticle surface modification with PEI, CP and PVP was verified with FTIR (Figure 2b, SI analysis). The CD core size determined by dynamic light scattering (DLS) was 1.7±0.7 nm with a range of size distributions (1.5 to 7.4 nm) similar to what we observed in TEM images (Figure S1). The hydrodynamic diameter was quantified by DLS for PEI-CD (4.3±1.5 nm), CP-CD (6.6±3.8 nm), and PVP-CD (4.3±1.9 nm) (Figure 2c). The average DLS size for all CDs was not significantly different (one-way ANOVA, $p > 0.05$) and there was a strong overlap in their size distribution (Figure 2c). There were no detectable free polymers in our CD suspensions based on CD mass change analysis after additional washing of CDs with DI water and comparisons of free polymer DLS with that of CDs (Figure S2). The PEI, CP and PVP surface coatings

of CD resulted in significantly different nanoparticle charges (one-way ANOVA, $p < 0.0001$) (Figure 2d). PEI-CD were highly positively charged with a zeta potential of 46.0±3.3 mV due to the abundant amine groups of the PEI polymer. In contrast, CP-CD had a highly negative zeta potential of -46.2±1.1 mV (Figure 2d) because of the surface modification with carboxylated PEI. PVP-CD showed a relatively neutral charge with a zeta potential of -8.6±1.3 mV (Figure 2d), which can be attributed to the polar carbonyl groups. All three CDs were strongly fluorescent upon excitation at 355 nm and exhibited similar emission profiles ranging from 400 to 600 nm with maxima at approximately 460 nm (Figure 2e). The similarities in CD optical properties were likely due to their fluorescence emission originating from the same CD core. The CD emission had almost no overlap with chloroplast autofluorescence (>650 nm). The distinct and separate emission windows allowed us to differentiate fluorescence signals from CD and chloroplasts during confocal microscopy imaging of nanoparticle treated plant and algae. PEI-CD and SA-CD exhibited a similar quantum yield of 0.4%, while PVP-CD showed the highest quantum yield of 1.7% (Table S1), which can be attributed to the passivation effect.[72] Together, our CD characterization analysis indicated carbon dots with varying surface coatings, similar size and fluorescence emission range, but different zeta potentials.

Native and model cell wall characterization. Extracted native Arabidopsis cell walls formed a patchy and rough surface on a glass substrate, similar to cellulose model cell walls whereas pectin distributed more uniformly over a planar surface (Figure 3a). AFM analysis of native cell walls also showed a patchy surface with average thickness of 80 ± 46 nm and model cell wall surfaces made of finely-networked fibers similar to those of plant cell walls.[73,74] The pectin model cell wall surface exhibited fibers forming a layer of 21 ± 7 nm whereas the cellulose model surface had 87 ± 69 nm in average thickness, respectively (Figure 3a, ANOVA $p > 0.5$). The FTIR analysis for native cell walls identified characteristic vibrational bands arising from carbohydrate cell wall components of pectin, cellulose,

hemicellulose, and lignin (Figure 3b-c, SI analysis).[75,76] XPS analysis of the C1s region of the model pectin layer formed on an SiO_2 QCM-D sensor indicated that pectin is largely composed of poly-D-galacturonic acid and methyl ester[77] (Figure S3), although other monomers can also be present both in model and native cell walls (Figure S4, SI analysis). The differences in pectin and cellulose functional groups are reflected in their zeta potentials. Both native and model cell wall surfaces had negative zeta potentials (10 mM TES buffer, 0.1 mM NaCl, pH 7.4) where pectin was more negatively charged (-54.9±1.1 mV) compared to cellulose (-20.6±1.6 mV) due to the presence of carboxyl groups in pectin ($p<0.0001$) (Figure 3d). The highly negative zeta potential of pectin is likely due to the abundant carboxyl groups as indicated in FTIR analysis (SI analysis),[78] while the hydroxyl groups on cellulose account for the relatively mild negative potential.[50]

Carbon dot interactions with native plant and algae cell walls. Isolated plant cell walls and algae cell walls treated with the positively charged PEI-CD exhibited a characteristic CD fluorescence signal in confocal microscopy images (Figure 4). In contrast, native cell walls exposed to PVP-CD and CP-CD did not have significant CD fluorescence emission, similar to native cell wall controls without nanoparticles (Figure S5, and S6). The PEI-CD were preferentially localized on the algae cell wall and cell membrane surrounding chloroplasts (Figure 4d). No CD fluorescence emission was detected in green algae cells exposed to PVP-CD or CP-CD, indicating low affinity of neutral and negatively charged nanoparticles to native algae cell walls (Figure S6). A comparison of integrated and normalized CD fluorescent intensity per area of native cell wall images collected by confocal microscopy indicated adsorption of only positively charged PEI-CD to native cell walls (one-way ANOVA, $p < 0.05$) (Figure 4b-c). Previous studies have indicated positively charged nanoparticle delivery to leaf mesophyll cells[31,79] or accumulation in roots likely due to their adhesion to cell walls.[34,35] whereas negatively charged nanoparticles preferentially translocate in vascular tissues.[38] The differences reported in uptake

between positive and negative charged nanoparticles in plant mesophyll, stomata guard cells, roots and vasculature could be due to variations in the content or arrangement of plant cell wall components (e.g. negatively charged pectin) or differences across plant species.[31,32,80,81]

Chemical interactions of model cell walls with carbon dots. Confocal fluorescence microscopy analysis indicated a stronger binding affinity of positively charged PEI-CD to pectin compared to cellulose model surfaces (Figure 5a). Pectin model cell walls exposed to PEI-CD displayed remarkably bright CD fluorescence across most of the model surface. In contrast, no CD fluorescence signal was detected for pectin model cell walls treated with negatively charged CP-CD and neutrally charged PVP-CD (Figure S7). The integrated and normalized CD fluorescence intensity over the imaged region was at least two orders of magnitude higher for pectin model cell walls exposed to PEI-CD than for CP-CD and PVP-CD (one-way ANOVA, $p < 0.001$) (Figure 5b). The PEI-CD fluorescence intensity observed in cellulose model surfaces was an order of magnitude lower compared to pectin counterparts (one-way ANOVA, $p < 0.001$) (Figure 5b) whereas no fluorescence signal was detected for cellulose surfaces treated with CP-CD and PVP-CD (Figure S8). Overall, the confocal microscopy analysis shows that positively charged PEI-CD strongly interacts with negatively charged pectin model cell wall surfaces and to a much smaller extent with cellulose surfaces.

To elucidate chemical interactions of nanoparticles with model cell wall surfaces, we performed FTIR analysis of pectin and cellulose surfaces interfaced with CD (Figure 6). The PEI-CD treated pectin model cell walls (Figure 6a) exhibited a significantly enhanced vibration band at 1605 cm^{-1} from deprotonated carboxylic acid groups relative to the band at 1736 cm^{-1} from esterified and protonated carboxylic acids present in pectin alone.[82–84] This indicates that the amine groups of PEI-CD deprotonated the carboxylic acid groups on pectin and formed ammonium cations. The ionic interactions

formed by the negatively charged carboxylate groups and positively charged ammonium cation groups can lead to strong binding between pectin model cell walls and PEI-CD. Although hydrogen bonding between amine molecules and pectin is possible, this interaction becomes significant at pH levels lower than those in this study.[85] On the other hand, no intensity change of the two vibration bands at 1736 and 1605 cm^{-1} was observed for pectin model cell walls interacted with CP-CD and PVP-CD (Figure 6a). Cellulose model surfaces exposed to all CD types showed no emerging vibration bands (Figure 6a) within the 1500 to 2000 cm^{-1} range containing characteristic FTIR signals for CD (Figure 2b). We expected a small amount of PEI-CD attached to cellulose but it is likely that this interaction is under the FTIR detection limit. FTIR analyses are consistent with confocal microscopy results indicating that only PEI-CD interact with model cell wall surfaces, and that the affinity of PEI-CD to pectin is significantly stronger than that to cellulose.

We collected XPS spectra (N 1s electron orbital) of cell wall model surfaces interfaced with CDs to elucidate the chemical bonding nature of their interactions (Figure 6b). Both pectin model cell walls and PEI-CD exhibited a binding energy at 399.6 eV, corresponding to the N 1s electrons in amide and amine groups.[86] This is consistent with FTIR analysis indicating the presence of amide and amine groups in pectin and PEI-CD, respectively. After being exposed to PEI-CD, the pectin model cell walls exhibited a new peak at 401.3 eV, which can be attributed to the N 1s electrons of positively charged quaternary ammonium cations.[86–88] This indicates that amine groups on PEI-CD were protonated by the carboxylic acids on pectin, resulting in the formation of quaternary ammonium cations. The positively charged ammonium cations form ionic bonds with deprotonated and negatively charged carboxyl groups, which may explain the strong affinity between PEI-CD and pectin observed in confocal microscopy images and FTIR spectra. In contrast, no changes were observed for the XPS spectra of pectin model cell walls after treatment with CP-CD and PVP-CD. As expected, the N 1s spectrum

(Figure 6b) for cellulose model cell walls without CD had no characteristic XPS peaks in the detected range due to the lack of nitrogen in cellulose.[89,90] Interestingly, the cellulose model cell walls exposed to PEI-CD showed an XPS peak from N 1s electrons, confirming the adsorption of PEI-CD to cellulose that we observed in confocal microscopy analysis. Peak deconvolution generated two subpeaks at a binding energy of 399.6 and 400.5 eV, which can be assigned to the N atoms of PEI-CD in pristine amine groups, and amine groups after forming hydrogen bonds (N···HO) with hydroxyl groups on cellulose.[91–93] The XPS peak from N 1s electrons was not observed for cellulose model surfaces interfaced with CP-CD or PVP-CD. The ionic bond observed between the amine and carboxyl groups of PEI-CD and pectin can be an order of magnitude stronger than that of the hydrogen bonds[94–96] between PEI-CD and cellulose, supporting our results that PEI-CD exhibit a higher binding affinity to pectin than cellulose model cell walls. Although hydrogen bonding may occur between CDs and cell walls, we only observed weak interactions of PEI-CD with model cellulose surfaces. Instead our FTIR and XPS analyses indicate a strong binding of PEI-CD to pectin via electrostatics (Figure 6).

We conducted additional FTIR analysis to examine the interaction between pectin model cell walls and PEI-CD with and without covalent conjugation and at different pH within the physiological range (5.5 to 7.4) to understand the role of hydrogen bonding, covalent bonding and electrostatics. FTIR analysis of O-H stretching for pectin model surfaces resulted in a blue-shift from 3268 cm^{-1} to 3388 cm^{-1} after exposure to PEI-CD indicating a decrease in hydrogen bonding[97] when the nanoparticles are exposed the pectin model cell wall surface (Figure S9a). There was no significant change in the O-H stretching peak within the plant physiological range of pH (5.5 to 7.4) (Figure S9b). Furthermore, the FTIR amide peak (1615 cm^{-1}) observed after intentional covalent conjugation by a coupling reaction between amine and carboxyl groups of PEI-CD and pectin was blue shifted and not observed in the PEI-CD interacted with pectin model cell walls without coupling reaction (1589 cm^{-1}) (Figure S9c). Changes

in pH from 7.4 to acidic 5.5 did not affect COO^- stretching (from 1589 to 1591 cm^{-1}) (Figure S9d). The pH did not affect COO^- or O-H stretching likely because this pH change was not below or above the pKa values for pectin (3.5) and PEI (8.1-9.9), respectively. Overall, these FTIR analysis support that there is minimal hydrogen bonding or covalent bonding between PEI-CD and pectin model cell walls, and that pH does not affect the electrostatic interactions of PEI-CD with pectin within the plant physiological range. These analyses also indicated that PEI-CD bind to pectin by reversible[98,99] electrostatic interactions between carboxylate anions and ammonium cations whereas cellulose interaction with PEI-CD is dominated by weaker hydrogen bonds between amine groups with hydroxyl groups (Figure 6c).

Real-time interactions of carbon dots with pectin model surfaces. To understand the strong interactions of PEI-CD with model pectin surfaces, we performed quartz crystal microbalance with dissipation monitoring (QCM-D) analysis (Figure 7). A pectin layer was built on SiO_2-coated QCM-D sensors by modifying a predeposited 3-aminopropyltriethoxysilane (APTS) layer on the sensor surface (Figure 7a).[100] The initial adsorption efficiencies on pectin model surfaces for the three CDs were in agreement with confocal microscopy, FTIR and XPS analysis. The PEI-CD had higher adsorption efficiency compared to that of CP-CD and PVP-CD (Figure 7b). Once CD interactions with the pectin model surfaces reached an equilibrium, the surface was rinsed with ultrapure water and the acoustic mass densities (Γ_{QCM-D}) of CDs on pectin were calculated by Eq.(2) to evidence attachment. Positively charged PEI-CD showed significantly more acoustic mass density on pectin model surfaces than CP-CD and PVP-CD (Figure 7c). The lack of interaction with negatively charged CP-CD after rinse supports the role of electrostatics determining interactions between positively charged PEI-CD and negatively charged pectin. The significantly smaller extent of neutrally charged PVP-CD adsorption to pectin ($p < 0.001$) after rinse can be attributed to deposition by gravity.[101] The acoustic mass density analysis

supports the role of electrostatics determining the interactions between positively charged PEI-CD and negatively charged pectin. We recently reported that CD interactions with lipid membranes from chloroplasts are also dictated by electrostatic interactions.[41] Similar to native and model plant cell walls, QCM-D analysis demonstrated that only the positively charged CD led to detectable attachment to chloroplast model and native membranes compared to their negative and neutral counterparts. Overall, the high adsorption affinity and acoustic mass density on the pectin layer upon exposure to PEI-CD support that electrostatics plays a key role in the interactions between positively charged nanoparticles and pectin model cell wall surfaces.

We constructed more complex model pectin model surfaces with calcium ions that play a critical role in maintaining and modifying cell wall structure by forming cross linking bonds with pectin hydrogels.[102] Calcium cations were added to pectin model cell walls as chloride salt at concentrations within the reported plant physiological range (0-1 mM).[103,104] Upon addition of Ca^{2+}, the adsorption efficiency of PEI-CD decreased from $3.4x10^{-9}$ (0 mM Ca^{2+}) to $7.8x10^{-10}$ (0.1 mM Ca^{2+}) and $1.1x10^{-9}$ (1 mM Ca^{2+}) (one-way ANOVA, $p < 0.05$) (Figure 7d). Given that calcium ions interact with carboxylate groups of pectin at the neutral pH conditions tested,[105,106] the addition of Ca^{2+} during model pectin layer construction was expected to permanently hinder the electrostatic interactions between PEI-CD and the pectin layer. However, this hindrance was only observed at the initial stage of PEI-CD interaction with the pectin layer. Upon the maximum adsorption of PEI-CD, Ca^{2+} did not lead to statistically significant differences on acoustic mass density (Figure 7e). The colloidal stability of PEI-CD in the presence of Ca^{2+} (Figure S10) was not a factor influencing these interactions with model pectin cell walls. The PEI-CD maintained a similar hydrodynamic size (3.4 to 4.1 nm) and charge (17.4 to 25.4 mV) within the Ca^{2+} concentration range used in this study (0 to 1 mM) (Figure S10). Confocal imaging, FTIR and XPS analysis also indicated that the electrostatic interactions of PEI-CD with carboxylate groups of pectin

were not affected within this range of Ca^{2+} concentrations. The PEI-CD fluorescence intensity per area of pectin model surfaces was similar from 0 to 1 mM Ca^{2+} (Figure S11a-c). FTIR analysis indicated similar characteristic vibration bands (1500 to 2000 cm^{-1}) from carboxylate groups of pectin model surfaces interfaced with PEI-CD at different Ca^{2+} concentrations. XPS analysis of the N1s electrons in amide and amine groups (399.6 eV) in the presence of Ca^{2+} indicated that the formation of quaternary ammonium cations between the amine groups of PEI-CDs and the carboxylic acids of pectin were not affected (Figure S11d). Interestingly, our previous study reports that CD attachment to model chloroplast membranes exhibited a different response to changes in ionic strength (KCl)[41] in a manner that is consistent with electrical double layer compression of CDs on plant lipid membranes. Overall, our results indicate that Ca^{2+} affects the initial absorption efficiency of positively charged PEI-CD to pectin surface but not their final accumulation on the model cell wall surface.

Role of carbon dot surface charge density on the interactions with cell walls. To probe the effect of nanoparticle surface charge using similar polymer coating composition, the CDs were coated with PEI polymers of different molecular weights (0.6k, 10k, and 25k) resulting in positively charged PEI-CD with varying densities of amine groups and surface charge densities (Figure 8a). The PEI 0.6k, 10k, and 25k CDs had similar absorption peaks at 250 nm and 355 nm and fluorescence emission spectra with peaks ranging from 400 to 550 nm (Figure 8b-c). All PEI-CD had a similar size based on AFM and DLS analysis ranging from 2.6±1.1, to 4.6±0.7 nm (one-way ANOVA, $p > 0.05$) in hydrodynamic diameter (Figure S12-13). Likewise, the zeta potentials for PEI 0.6k, 10k, and 25k CDs were not different from each other ($p > 0.05$) and were within a narrow range of 20.7±5.5 and 27.0±9.7 mV (Figure 8d). Characterization of the surface charge density of PEI-CD by a polyelectrolyte titration method[107] indicated that PEI 0.6k CD had the highest surface charge density (8 μmol/mg) whereas the PEI 10k CDs showed the lowest (2 μmol/mg) (Figure 8e). We tested PEI 0.6k, 10k, and 25k CDs binding to

Arabidopsis native cell wall surfaces by confocal imaging and observed the highest CD fluorescence intensity from the cell wall surfaces exposed to the PEI-CD 0.6k having the largest surface charge density (Figure 8f). The average CD fluorescence intensity per unit area increased steadily with the surface charge density of PEI-CD (One-way ANOVA, $p < 0.05$) (Figure 8g). These order of magnitude differences were not explained by the fluorescence quantum yield of PEI-CDs with different surface charge density ranging from 10.6% to 16.7% (Table S1) where the lowest quantum yield corresponded to the PEI-CD with highest surface charge density (PEI 0.6k). Furthermore, confocal imaging analyses of fluorescence intensity were normalized by the quantum yield of CDs for comparison. These results indicate that enhancing nanoparticle surface charge density strengthens their interactions with plant cell wall surfaces. They offer a pathway to design nanomaterials with modulated binding affinity to plant cell walls. A recent study in mammalian cells that lack cell walls, observed that nanoparticle surface charge densities are a stronger indicator of toxicity to cells than zeta potentials.[107] Our study points out that surface charge density is a factor for controlling the interactions of nanoparticles with cell walls for sustainable agriculture applications with reduced impact on the environment.

Environmental implications. We developed novel model surfaces for assessing the interactions of nanomaterials with plant and algae cell walls, a main barrier for translocation of nanomaterials in these photosynthetic organisms that support life on earth. Model cell walls built with the main components of native cell walls (pectin and cellulose) were used to study their interactions with fluorescent CDs of different surface charge. This approach allowed us to elucidate chemical mechanisms underlying the role of electrostatics on the interactions between the plant cell walls and nanoparticles. Amine functional groups on PEI-CD surface formed strong ionic bonding with abundant carboxylic acid groups of the pectin model surfaces. In contrast, PEI-CD formed weaker hydrogen bonding with hydroxyl groups of cellulose model surfaces. Real-time monitoring analysis indicated that the presence of Ca^{2+} in cell walls

affects the initial absorption efficiency of positively charged nanoparticles to pectin surface but not their final accumulation on the cell wall surface. Furthermore, increasing the surface charge density of positively charged PEI-CD enhances their interactions with cell walls providing an approach to tune nanoparticle binding and translocation. This study indicates that electrostatic interactions of nanoparticles with pectin and nanoparticle surface charge density determine the translocation of nanoparticles across plant and algae cell walls. Elucidating rules for controlling the interactions of nanomaterials with photosynthetic organism biosurfaces will be crucial for designing targeted and controlled delivery of chemicals and biomolecule cargoes enabled by nanotechnology.

We elucidated mechanisms of nanomaterial interactions with plant and algae cell wall components (pectin and cellulose) focusing on the role of electrostatic and hydrogen bonding interactions. We validated these results with real cell walls demonstrating that our approach can provide mechanistic insight, chemical and quantitative analyses that would not be possible with more complex real cell walls. Understanding the underlying mechanisms of nanomaterial-cell wall interactions using model surfaces will be instrumental to determine how other properties such as size, morphology, hydrophobicity,[31,32] affect binding, translocation and distribution of nanomaterials in plant and algae interfaces in the environment. In addition, model cell wall surfaces can serve as tools to understand how transformations of nanomaterials (e.g. corona formation and dissolution) influence their binding and translocation at the cell wall interface. Future research will elucidate how heterogeneity in cell wall composition affects interactions with nanoparticles. This will require a more precise tuning of the composition of pectin and cellulose cell wall model surfaces. More realistic and tunable cell wall model surfaces can advance our understanding of the physical and chemical interactions with plant and algae cell walls.

A more sustainable agriculture will require nanomaterials that are scalable, economical, with low environmental footprint.[108] In this study, we used carbon dots that can be manufactured in large scale through simple bottom up approaches,[63] using abundant, low cost, and renewable resources such as animal and plant derivatives.[109] Future research efforts should address cell wall interactions with more reactive nanomaterials such as complex metal oxides that can experience larger transformations due to dissolution or redox chemistry processes and consider the role of nanoparticle charge in the formation of biomolecule coronas from plants and microorganism membranes.[110,111] Determining the role of nanomaterial properties on the interactions with biosurfaces of photosynthetic organisms will allow us to develop sustainable nanotechnology-based tools for addressing the challenge of improving food security and production while reducing the impact of agriculture on the environment.

ASSOCIATED CONTENT

Corresponding Author

Juan Pablo Giraldo - *Department of Botany and Plant Sciences, University of California Riverside, Riverside, California, 92521, United States; Email: juanpablo.giraldo@ucr.edu*

Authors

Su-Ji Jeon - *Department of Botany and Plant Sciences, University of California Riverside, Riverside, California, 92521, United States*

Peiguang Hu - *Department of Botany and Plant Sciences, University of California Riverside, Riverside, California, 92521, United States*

Kyoungtea Kim - *Molecular and Environmental Toxicology, University of Wisconsin—Madison, Madison, Wisconsin* 53706, United States

Caroline M. Anastasia -*Department of Chemistry, Johns Hopkins University, Baltimore, Maryland 21218, United States*

Hye-In Kim - *Department of Botany and Plant Sciences, University of California Riverside, Riverside, California, 92521, United States*

Christopher Castillo - *Department of Botany and Plant Sciences, University of California Riverside, Riverside, California, 92521, United States*

Colleen Ahern - *Department of Botany and Plant Sciences, University of California Riverside, Riverside, California, 92521, United States*

Joel A. Pedersen - *Molecular and Environmental Toxicology, University of Wisconsin—Madison, Madison, Wisconsin 53706, United States, Department of Environmental Health and Engineering, Johns Hopkins University, Baltimore, Maryland 21218, United States*

Howard Fairbrother - *Department of Chemistry, Johns Hopkins University, Baltimore, Maryland 21218, United States*

Notes

The authors declare no competing financial interests.

Acknowledgements

This work was supported by the National Science Foundation under the Center for Sustainable Nanotechnology, CHE-2001611. The CSN is part of the Centers for Chemical Innovation Program. XPS measurements were performed using the Kratos AXIS ULTRA DLD XPS system which is supported by NSF DMR-0958796. Schematic figures were created with BioRender.com.

Supplementary information

Information about carbon dot FTIR analysis, FTIR and XPS analysis of native and model cell walls; materials and methods for model cell wall synthesis and characterization, CD synthesis and characterization, relative quantum yield of CDs, plant and algae growth, Isolation of *Arabidopsis* plant cell walls, CD interactions with isolated plant cell walls, green algae interactions with CD *in vivo,* XPS functional group analysis of cell wall surfaces, pectin model surfaces on QCM-D sensors; and figures S1-S13.

REFERENCES

(1) *World Population Prospects: The 2017 Revision, Key Findings and Advance Tables*; United Nations, 2017.
(2) Lowry, G. V.; Avellan, A.; Gilbertson, L. M. Opportunities and Challenges for Nanotechnology in the Agri-Tech Revolution. *Nat. Nanotechnol.* **2019**, *14* (6), 517–522.
(3) van Dijk, M.; Morley, T.; Rau, M. L.; Saghai, Y. A Meta-Analysis of Projected Global Food Demand and Population at Risk of Hunger for the Period 2010-2050. *Nat Food* **2021**, *2* (7), 494–501.
(4) Kah, M.; Tufenkji, N.; White, J. C. Nano-Enabled Strategies to Enhance Crop Nutrition and Protection. *Nat. Nanotechnol.* **2019**, *14* (6), 532–540.
(5) Intergovernmental Panel on Climate Change (IPCC). Food Security. In *Climate Change and Land: IPCC Special Report on Climate Change, Desertification, Land Degradation, Sustainable Land Management, Food Security, and Greenhouse Gas Fluxes in Terrestrial Ecosystems*; Cambridge University Press, 2022; pp 437–550.
(6) Landry, M. P.; Mitter, N. How Nanocarriers Delivering Cargos in Plants Can Change the GMO Landscape. *Nat. Nanotechnol.* **2019**, *14* (6), 512–514.
(7) Demirer, G. S.; Zhang, H.; Matos, J. L.; Goh, N. S.; Cunningham, F. J.; Sung, Y.; Chang, R.; Aditham, A. J.; Chio, L.; Cho, M.-J.; Staskawicz, B.; Landry, M. P. High Aspect Ratio Nanomaterials Enable Delivery of Functional Genetic Material without DNA Integration in Mature Plants. *Nat. Nanotechnol.* **2019**, *14* (5), 456–464.
(8) Demirer, G. S.; Zhang, H.; Goh, N. S.; Pinals, R. L.; Chang, R.; Landry, M. P. Carbon Nanocarriers Deliver siRNA to Intact Plant Cells for Efficient Gene Knockdown. *Sci Adv* **2020**, *6* (26), eaaz0495.
(9) Zhang, H.; Goh, N. S.; Wang, J. W.; Pinals, R. L.; González-Grandío, E.; Demirer, G. S.; Butrus, S.; Fakra, S. C.; Del Rio Flores, A.; Zhai, R.; Zhao, B.; Park, S.-J.; Landry, M. P. Nanoparticle Cellular Internalization Is Not Required for RNA Delivery to Mature Plant Leaves. *Nat. Nanotechnol.* **2021**. https://doi.org/10.1038/s41565-021-01018-8.
(10) Kwak, S.-Y.; Lew, T. T. S.; Sweeney, C. J.; Koman, V. B.; Wong, M. H.; Bohmert-Tatarev, K.; Snell, K. D.; Seo, J. S.; Chua, N.-H.; Strano, M. S. Chloroplast-Selective Gene Delivery and Expression in Planta Using Chitosan-Complexed Single-Walled Carbon Nanotube Carriers. *Nat. Nanotechnol.* **2019**, *14* (5), 447–455.
(11) Sekhon, B. S. Nanotechnology in Agri-Food Production: An Overview. *Nanotechnol. Sci. Appl.* **2014**, *7*,

31–53.
(12) White, J. C.; Gardea-Torresdey, J. Achieving Food Security through the Very Small. *Nat. Nanotechnol.* **2018**, *13* (8), 627–629.
(13) Xu, T.; Ma, C.; Aytac, Z.; Hu, X.; Ng, K. W.; White, J. C.; Demokritou, P. Enhancing Agrichemical Delivery and Seedling Development with Biodegradable, Tunable, Biopolymer-Based Nanofiber Seed Coatings. *ACS Sustainable Chem. Eng.* **2020**, *8* (25), 9537–9548.
(14) Chariou, P. L.; Ma, Y.; Hensley, M.; Rosskopf, E. N.; Hong, J. C.; Charudattan, R.; Steinmetz, N. F. Inactivated Plant Viruses as an Agrochemical Delivery Platform. *ACS Agric. Sci. Technol.* **2021**, *1* (3), 124–130.
(15) Giraldo, J. P.; Wu, H.; Newkirk, G. M.; Kruss, S. Nanobiotechnology Approaches for Engineering Smart Plant Sensors. *Nat. Nanotechnol.* **2019**, *14* (6), 541–553.
(16) Wu, H.; Nißler, R.; Morris, V.; Herrmann, N.; Hu, P.; Jeon, S.-J.; Kruss, S.; Giraldo, J. P. Monitoring Plant Health with Near-Infrared Fluorescent H2O2 Nanosensors. *Nano Lett.* **2020**, *20* (4), 2432–2442.
(17) Lew, T. T. S.; Koman, V. B.; Silmore, K. S.; Seo, J. S.; Gordiichuk, P.; Kwak, S.-Y.; Park, M.; Ang, M. C.-Y.; Khong, D. T.; Lee, M. A.; Chan-Park, M. B.; Chua, N.-H.; Strano, M. S. Real-Time Detection of Wound-Induced H2O2 Signalling Waves in Plants with Optical Nanosensors. *Nat Plants* **2020**, *6* (4), 404–415.
(18) Hofmann, T.; Lowry, G. V.; Ghoshal, S.; Tufenkji, N.; Brambilla, D.; Dutcher, J. R.; Gilbertson, L. M.; Giraldo, J. P.; Kinsella, J. M.; Landry, M. P.; Lovell, W.; Naccache, R.; Paret, M.; Pedersen, J. A.; Unrine, J. M.; White, J. C.; Wilkinson, K. J. Technology Readiness and Overcoming Barriers to Sustainably Implement Nanotechnology-Enabled Plant Agriculture. *Nature Food* **2020**, *1* (7), 416–425.
(19) Wang, P.; Lombi, E.; Zhao, F.-J.; Kopittke, P. M. Nanotechnology: A New Opportunity in Plant Sciences. *Trends Plant Sci.* **2016**, *21* (8), 699–712.
(20) Wang, D.; Saleh, N. B.; Byro, A.; Zepp, R.; Sahle-Demessie, E.; Luxton, T. P.; Ho, K. T.; Burgess, R. M.; Flury, M.; White, J. C.; Su, C. Nano-Enabled Pesticides for Sustainable Agriculture and Global Food Security. *Nat. Nanotechnol.* **2022**. https://doi.org/10.1038/s41565-022-01082-8.
(21) Squire, H. J.; Tomatz, S.; Voke, E.; González-Grandío, E.; Landry, M. The Emerging Role of Nanotechnology in Plant Genetic Engineering. *Nature Reviews Bioengineering* **2023**, 1–15.
(22) Popper, Z. A.; Michel, G.; Hervé, C.; Domozych, D. S.; Willats, W. G. T.; Tuohy, M. G.; Kloareg, B.; Stengel, D. B. Evolution and Diversity of Plant Cell Walls: From Algae to Flowering Plants. *Annu. Rev. Plant Biol.* **2011**, *62*, 567–590.
(23) Schwab, F.; Zhai, G.; Kern, M.; Turner, A.; Schnoor, J. L.; Wiesner, M. R. Barriers, Pathways and Processes for Uptake, Translocation and Accumulation of Nanomaterials in Plants – Critical Review. *Nanotoxicology* **2016**, *10* (3), 257–278.
(24) Nolte, T. M.; Hartmann, N. B.; Kleijn, J. M.; Garnæs, J.; van de Meent, D.; Jan Hendriks, A.; Baun, A. The Toxicity of Plastic Nanoparticles to Green Algae as Influenced by Surface Modification, Medium Hardness and Cellular Adsorption. *Aquat. Toxicol.* **2017**, *183*, 11–20.
(25) Kosak, L. A.; Brandt, T.; Sigg, L.; Behra, R. Uptake and Effects of cerium(III) and Cerium Oxide Nanoparticles to Chlamydomonas Reinhardtii. *Aquat. Toxicol.* **2018**, *197*, 41–46.
(26) Santana, I.; Jeon, S.-J.; Kim, H.-I.; Islam, M. R.; Castillo, C.; Garcia, G. F. H.; Newkirk, G. M.; Giraldo, J. P. Targeted Carbon Nanostructures for Chemical and Gene Delivery to Plant Chloroplasts. *ACS Nano* **2022**. https://doi.org/10.1021/acsnano.2c02714.
(27) Newkirk, G. M.; de Allende, P.; Jinkerson, R. E.; Giraldo, J. P. Nanotechnology Approaches for Chloroplast Biotechnology Advancements. *Front. Plant Sci.* **2021**, *12*, 691295.
(28) Kumar, S.; Nehra, M.; Dilbaghi, N.; Marrazza, G.; Tuteja, S. K.; Kim, K.-H. Nanovehicles for Plant Modifications towards Pest- and Disease-Resistance Traits. *Trends Plant Sci.* **2019**. https://doi.org/10.1016/j.tplants.2019.10.007.
(29) Wong, M. H.; Misra, R. P.; Giraldo, J. P.; Kwak, S.-Y.; Son, Y.; Landry, M. P.; Swan, J. W.; Blankschtein, D.; Strano, M. S. Lipid Exchange Envelope Penetration (LEEP) of Nanoparticles for Plant Engineering: A Universal Localization Mechanism. *Nano Lett.* **2016**, *16* (2), 1161–1172.
(30) Lew, T. T. S.; Wong, M. H.; Kwak, S.-Y.; Sinclair, R.; Koman, V. B.; Strano, M. S. Rational Design

Principles for the Transport and Subcellular Distribution of Nanomaterials into Plant Protoplasts. *Small* **2018**, *14* (44), e1802086.
(31) Hu, P.; An, J.; Faulkner, M. M.; Wu, H.; Li, Z.; Tian, X.; Giraldo, J. P. Nanoparticle Charge and Size Control Foliar Delivery Efficiency to Plant Cells and Organelles. *ACS Nano* **2020**, *14* (7), 7970–7986.
(32) Avellan, A.; Yun, J.; Zhang, Y.; Spielman-Sun, E.; Unrine, J. M.; Thieme, J.; Li, J.; Lombi, E.; Bland, G.; Lowry, G. V. Nanoparticle Size and Coating Chemistry Control Foliar Uptake Pathways, Translocation, and Leaf-to-Rhizosphere Transport in Wheat. *ACS Nano* **2019**, *13* (5), 5291–5305.
(33) Slomberg, D. L.; Schoenfisch, M. H. Silica Nanoparticle Phytotoxicity to Arabidopsis Thaliana. *Environ. Sci. Technol.* **2012**, *46* (18), 10247–10254.
(34) Zhu, Z.-J.; Wang, H.; Yan, B.; Zheng, H.; Jiang, Y.; Miranda, O. R.; Rotello, V. M.; Xing, B.; Vachet, R. W. Effect of Surface Charge on the Uptake and Distribution of Gold Nanoparticles in Four Plant Species. *Environ. Sci. Technol.* **2012**, *46* (22), 12391–12398.
(35) Spielman-Sun, E.; Lombi, E.; Donner, E.; Howard, D.; Unrine, J. M.; Lowry, G. V. Impact of Surface Charge on Cerium Oxide Nanoparticle Uptake and Translocation by Wheat (Triticum Aestivum). *Environ. Sci. Technol.* **2017**, *51* (13), 7361–7368.
(36) Zhang, Y.; Fu, L.; Li, S.; Yan, J.; Sun, M.; Giraldo, J. P.; Matyjaszewski, K.; Tilton, R. D.; Lowry, G. V. Star Polymer Size, Charge Content, and Hydrophobicity Affect Their Leaf Uptake and Translocation in Plants. *Environ. Sci. Technol.* **2021**, *55* (15), 10758–10768.
(37) Avellan, A.; Yun, J.; Morais, B. P.; Clement, E. T.; Rodrigues, S. M.; Lowry, G. V. Critical Review: Role of Inorganic Nanoparticle Properties on Their Foliar Uptake and in Planta Translocation. *Environ. Sci. Technol.* **2021**, *55* (20), 13417–13431.
(38) Su, Y.; Ashworth, V. E. T. M.; Geitner, N. K.; Wiesner, M. R.; Ginnan, N.; Rolshausen, P.; Roper, C.; Jassby, D. Delivery, Fate, and Mobility of Silver Nanoparticles in Citrus Trees. *ACS Nano* **2020**, *14* (3), 2966–2981.
(39) Chwalibog, A.; Sawosz, E.; Hotowy, A.; Szeliga, J.; Mitura, S.; Mitura, K.; Grodzik, M.; Orlowski, P.; Sokolowska, A. Visualization of Interaction between Inorganic Nanoparticles and Bacteria or Fungi. *Int. J. Nanomedicine* **2010**, *5*, 1085–1094.
(40) Zhang, W.; Stack, A. G.; Chen, Y. Interaction Force Measurement between E. Coli Cells and Nanoparticles Immobilized Surfaces by Using AFM. *Colloids Surf. B Biointerfaces* **2011**, *82* (2), 316–324.
(41) Kim, K.; Jeon, S.-J.; Hu, P.; Anastasia, C. M.; Beimers, W. F.; Giraldo, J. P.; Pedersen, J. A. Sulfolipid Density Dictates the Extent of Carbon Nanodot Interaction with Chloroplast Membranes. *Environ. Sci.: Nano* **2022**, *9* (8), 2691–2703.
(42) Pelaz, B.; del Pino, P.; Maffre, P.; Hartmann, R.; Gallego, M.; Rivera-Fernández, S.; de la Fuente, J. M.; Nienhaus, G. U.; Parak, W. J. Surface Functionalization of Nanoparticles with Polyethylene Glycol: Effects on Protein Adsorption and Cellular Uptake. *ACS Nano* **2015**, *9* (7), 6996–7008.
(43) Wilhelm, C.; Gazeau, F.; Roger, J.; Pons, J. N.; Bacri, J.-C. Interaction of Anionic Superparamagnetic Nanoparticles with Cells: Kinetic Analyses of Membrane Adsorption and Subsequent Internalization. *Langmuir* **2002**, *18* (21), 8148–8155.
(44) Fang, H. H.; Chan, K. Y.; Xu, L. C. Quantification of Bacterial Adhesion Forces Using Atomic Force Microscopy (AFM). *J. Microbiol. Methods* **2000**, *40* (1), 89–97.
(45) Horie, M.; Kato, H.; Iwahashi, H. Cellular Effects of Manufactured Nanoparticles: Effect of Adsorption Ability of Nanoparticles. *Arch. Toxicol.* **2013**, *87* (5), 771–781.
(46) Luo, J.; Chan, W.-B.; Wang, L.; Zhong, C.-J. Probing Interfacial Interactions of Bacteria on Metal Nanoparticles and Substrates with Different Surface Properties. *Int. J. Antimicrob. Agents* **2010**, *36* (6), 549–556.
(47) Chebli, Y.; Bidhendi, A. J.; Kapoor, K.; Geitmann, A. Cytoskeletal Regulation of Primary Plant Cell Wall Assembly. *Curr. Biol.* **2021**, *31* (10), R681–R695.
(48) Houston, K.; Tucker, M. R.; Chowdhury, J.; Shirley, N.; Little, A. The Plant Cell Wall: A Complex and Dynamic Structure As Revealed by the Responses of Genes under Stress Conditions. *Front. Plant Sci.* **2016**, *7*, 984.
(49) Keegstra, K. Plant Cell Walls. *Plant Physiol.* **2010**, *154* (2), 483–486.

(50) Stana-Kleinschek, K.; Ribitsch, V. Electrokinetic Properties of Processed Cellulose Fibers. *Colloids Surf. A Physicochem. Eng. Asp.* **1998**, *140* (1), 127–138.
(51) Voragen, A. G. J.; Coenen, G.-J.; Verhoef, R. P.; Schols, H. A. Pectin, a Versatile Polysaccharide Present in Plant Cell Walls. *Struct. Chem.* **2009**, *20* (2), 263.
(52) Celus, M.; Kyomugasho, C.; Van Loey, A. M.; Grauwet, T.; Hendrickx, M. E. Influence of Pectin Structural Properties on Interactions with Divalent Cations and Its Associated Functionalities. *Compr. Rev. Food Sci. Food Saf.* **2018**, *17* (6), 1576–1594.
(53) Shomer, I.; Novacky, A. J.; Pike, S. M.; Yermiyahu, U.; Kinraide, T. B. Electrical Potentials of Plant Cell Walls in Response to the Ionic Environment. *Plant Physiol.* **2003**, *133* (1), 411–422.
(54) Meychik, N. R.; Yermakov, I. P. Ion Exchange Properties of Plant Root Cell Walls. *Plant Soil* **2001**, *234* (2), 181–193.
(55) Zhang, M.; Hu, L.; Wang, H.; Song, Y.; Liu, Y.; Li, H.; Shao, M.; Huang, H.; Kang, Z. One-Step Hydrothermal Synthesis of Chiral Carbon Dots and Their Effects on Mung Bean Plant Growth. *Nanoscale* **2018**, *10* (26), 12734–12742.
(56) Wang, H.; Zhang, M.; Song, Y.; Li, H.; Huang, H.; Shao, M.; Liu, Y.; Kang, Z. Carbon Dots Promote the Growth and Photosynthesis of Mung Bean Sprouts. *Carbon N. Y.* **2018**, *136*, 94–102.
(57) Wang, A.; Kang, F.; Wang, Z.; Shao, Q.; Li, Z.; Zhu, G.; Lu, J.; Li, Y. Y. Facile Synthesis of Nitrogen-Rich Carbon Dots as Fertilizers for Mung Bean Sprouts. *Adv. Sustain. Syst.* **2019**, *3* (3), 1800132.
(58) Li, Y.; Xu, X.; Wu, Y.; Zhuang, J.; Zhang, X.; Zhang, H.; Lei, B.; Hu, C.; Liu, Y. A Review on the Effects of Carbon Dots in Plant Systems. *Materials Chemistry Frontiers* **2020**, *4* (2), 437–448.
(59) Li, H.; Huang, J.; Lu, F.; Liu, Y.; Song, Y.; Sun, Y.; Zhong, J.; Huang, H.; Wang, Y.; Li, S.; Lifshitz, Y.; Lee, S.-T.; Kang, Z. Impacts of Carbon Dots on Rice Plants: Boosting the Growth and Improving the Disease Resistance. *ACS Appl Bio Mater* **2018**, *1* (3), 663–672.
(60) Li, H.; Sun, C.; Vijayaraghavan, R.; Zhou, F.; Zhang, X.; MacFarlane, D. R. Long Lifetime Photoluminescence in N, S Co-Doped Carbon Quantum Dots from an Ionic Liquid and Their Applications in Ultrasensitive Detection of Pesticides. *Carbon N. Y.* **2016**, *104*, 33–39.
(61) Shi, X.; Wei, W.; Fu, Z.; Gao, W.; Zhang, C.; Zhao, Q.; Deng, F.; Lu, X. Review on Carbon Dots in Food Safety Applications. *Talanta* **2019**, *194*, 809–821.
(62) Ashrafi Tafreshi, F.; Fatahi, Z.; Ghasemi, S. F.; Taherian, A.; Esfandiari, N. Ultrasensitive Fluorescent Detection of Pesticides in Real Sample by Using Green Carbon Dots. *PLoS One* **2020**, *15* (3), e0230646.
(63) Đorđević, L.; Arcudi, F.; Cacioppo, M.; Prato, M. A Multifunctional Chemical Toolbox to Engineer Carbon Dots for Biomedical and Energy Applications. *Nat. Nanotechnol.* **2022**, *17* (2), 112–130.
(64) Delwiche, C. F.; Graham, L. E.; Thomson, N. Lignin-like Compounds and Sporopollenin Coleochaete, an Algal Model for Land Plant Ancestry. *Science* **1989**, *245* (4916), 399–401.
(65) Dixon, M. C. Quartz Crystal Microbalance with Dissipation Monitoring: Enabling Real-Time Characterization of Biological Materials and Their Interactions. *J. Biomol. Tech.* **2008**, *19* (3), 151–158.
(66) Reviakine, I.; Johannsmann, D.; Richter, R. P. Hearing What You Cannot See and Visualizing What You Hear: Interpreting Quartz Crystal Microbalance Data from Solvated Interfaces. *Anal. Chem.* **2011**, *83* (23), 8838–8848.
(67) Kankare, J. Sauerbrey Equation of Quartz Crystal Microbalance in Liquid Medium. *Langmuir* **2002**, *18* (18), 7092–7094.
(68) Jacobson, K. H.; Gunsolus, I. L.; Kuech, T. R.; Troiano, J. M.; Melby, E. S.; Lohse, S. E.; Hu, D.; Chrisler, W. B.; Murphy, C. J.; Orr, G.; Geiger, F. M.; Haynes, C. L.; Pedersen, J. A. Lipopolysaccharide Density and Structure Govern the Extent and Distance of Nanoparticle Interaction with Actual and Model Bacterial Outer Membranes. *Environ. Sci. Technol.* **2015**, *49* (17), 10642–10650.
(69) Mensch, A. C.; Hernandez, R. T.; Kuether, J. E.; Torelli, M. D.; Feng, Z. V.; Hamers, R. J.; Pedersen, J. A. Natural Organic Matter Concentration Impacts the Interaction of Functionalized Diamond Nanoparticles with Model and Actual Bacterial Membranes. *Environ. Sci. Technol.* **2017**, *51* (19), 11075–11084.
(70) Zhang, M.; Soto-Rodríguez, J.; Chen, I.-C.; Akbulut, M. Adsorption and Removal Dynamics of Polymeric Micellar Nanocarriers Loaded with a Therapeutic Agent on Silica Surfaces. *Soft Matter* **2013**, *9* (42), 10155–10164.

(71) Zhang, M.; Akbulut, M. Adsorption, Desorption, and Removal of Polymeric Nanomedicine on and from Cellulose Surfaces: Effect of Size. *Langmuir* **2011**, *27* (20), 12550–12559.
(72) Tachikawa, S.; Noguchi, A.; Tsuge, T.; Hara, M.; Odawara, O.; Wada, H. Optical Properties of ZnO Nanoparticles Capped with Polymers. *Materials* **2011**, *4* (6), 1132–1143.
(73) Zhang, Y.; Yu, J.; Wang, X.; Durachko, D. M.; Zhang, S.; Cosgrove, D. J. Molecular Insights into the Complex Mechanics of Plant Epidermal Cell Walls. *Science* **2021**, *372* (6543), 706–711.
(74) Gow, N. A. R.; Besra, G.; Bulone, V.; Carrington, M.; Höfte, H. The Cell Surface – A New Journal for Transkingdom Cell Wall Research. *The Cell Surface*. 2018, p 1. https://doi.org/10.1016/j.tcsw.2017.05.001.
(75) Kenđel, A.; Zimmermann, B. Chemical Analysis of Pollen by FT-Raman and FTIR Spectroscopies. *Front. Plant Sci.* **2020**, *11*, 352.
(76) Bhagia, S.; Ďurkovič, J.; Lagaňa, R.; Kardošová, M.; Kačík, F.; Cernescu, A.; Schäfer, P.; Yoo, C. G.; Ragauskas, A. J. Nanoscale FTIR and Mechanical Mapping of Plant Cell Walls for Understanding Biomass Deconstruction. *ACS Sustainable Chem. Eng.* **2022**, *10* (9), 3016–3026.
(77) Daas, P. J.; Boxma, B.; Hopman, A. M.; Voragen, A. G.; Schols, H. A. Nonesterified Galacturonic Acid Sequence Homology of Pectins. *Biopolymers* **2001**, *58* (1), 1–8.
(78) Opanasopit, P.; Apirakaramwong, A.; Ngawhirunpat, T.; Rojanarata, T.; Ruktanonchai, U. Development and Characterization of Pectinate Micro/nanoparticles for Gene Delivery. *AAPS PharmSciTech* **2008**, *9* (1), 67–74.
(79) Zhu, J.; Wang, J.; Zhan, X.; Li, A.; White, J. C.; Gardea-Torresdey, J. L.; Xing, B. Role of Charge and Size in the Translocation and Distribution of Zinc Oxide Particles in Wheat Cells. *ACS Sustainable Chem. Eng.* **2021**, *9* (34), 11556–11564.
(80) Cosgrove, D. J. Building an Extensible Cell Wall. *Plant Physiol.* **2022**, *189* (3), 1246–1277.
(81) Hafren, J.; Daniel, G.; Westernark, U. The Distribution of Acidic and Esterfied Pectin in Cambium, Developing Xylem and Mature Xylem of Pinnus Sylvestris. *IAWA J.* **2000**, *21*, 157–168.
(82) Manrique, G. D.; Lajolo, F. M. FT-IR Spectroscopy as a Tool for Measuring Degree of Methyl Esterification in Pectins Isolated from Ripening Papaya Fruit. *Postharvest Biol. Technol.* **2002**, *25* (1), 99–107.
(83) Iqbal, M.; Saeed, A.; Zafar, S. I. FTIR Spectrophotometry, Kinetics and Adsorption Isotherms Modeling, Ion Exchange, and EDX Analysis for Understanding the Mechanism of Cd(2+) and Pb(2+) Removal by Mango Peel Waste. *J. Hazard. Mater.* **2009**, *164* (1), 161–171.
(84) Cui, Y.; Chen, J.; Zhang, S. The Effect of Degree of Esterification of Pectin on the Interaction between Pectin and Wheat Gluten Protein. *Food Hydrocoll.* **2023**, *136*, 108272.
(85) Feng, S.; Yi, J.; Ma, Y.; Bi, J. The Role of Amide Groups in the Mechanism of Acid-Induced Pectin Gelation: A Potential pH-Sensitive Hydrogel Based on Hydrogen Bond Interactions. *Food Hydrocoll.* **2023**, *141*, 108741.
(86) Jansen, R. J. J.; van Bekkum, H. XPS of Nitrogen-Containing Functional Groups on Activated Carbon. *Carbon N. Y.* **1995**, *33* (8), 1021–1027.
(87) Schmiers, H.; Friebel, J.; Streubel, P.; Hesse, R.; Köpsel, R. Change of Chemical Bonding of Nitrogen of Polymeric N-Heterocyclic Compounds during Pyrolysis. *Carbon N. Y.* **1999**, *37* (12), 1965–1978.
(88) Cao, W.; Wang, Z.; Zeng, Q.; Shen, C. 13C NMR and XPS Characterization of Anion Adsorbent with Quaternary Ammonium Groups Prepared from Rice Straw, Corn Stalk and Sugarcane Bagasse. *Appl. Surf. Sci.* **2016**, *389*, 404–410.
(89) Pertile, R. A. N.; Andrade, F. K.; Alves, C.; Gama, M. Surface Modification of Bacterial Cellulose by Nitrogen-Containing Plasma for Improved Interaction with Cells. *Carbohydr. Polym.* **2010**, *82* (3), 692–698.
(90) Deslandes, Y.; Pleizier, G.; Poiré, E.; Sapieha, S.; Wertheimer, M. R.; Sacher, E. The Surface Modification of Pure Cellulose Paper Induced by Low-Pressure Nitrogen Plasma Treatment. *Plasmas Polym.* **1998**, *3* (2), 61–76.
(91) Kerber, S. J.; Bruckner, J. J.; Wozniak, K.; Seal, S.; Hardcastle, S.; Barr, T. L. The Nature of Hydrogen in X-ray Photoelectron Spectroscopy: General Patterns from Hydroxides to Hydrogen Bonding. *J. Vac. Sci.*

Technol. A **1996**, *14* (3), 1314–1320.
(92) Stevens, J. S.; Byard, S. J.; Seaton, C. C.; Sadiq, G.; Davey, R. J.; Schroeder, S. L. M. Proton Transfer and Hydrogen Bonding in the Organic Solid State: A Combined XRD/XPS/ssNMR Study of 17 Organic Acid–base Complexes. *Phys. Chem. Chem. Phys.* **2014**, *16* (3), 1150–1160.
(93) Spencer, J. N.; Wolbach, W. S.; Hovick, J. W.; Ansel, L.; Modarress, K. J. Hydrogen Bonding by Alcohols and Amines. *J. Solution Chem.* **1985**, *14* (11), 805–814.
(94) Steed, J. W.; Atwood, J. L. *Supramolecular Chemistry*; John Wiley & Sons, 2013.
(95) Faul, C. F. J.; Antonietti, M. Ionic Self-Assembly: Facile Synthesis of Supramolecular Materials. *Adv. Mater.* **2003**, *15* (9), 673–683.
(96) Hoeben, F. J. M.; Jonkheijm, P.; Meijer, E. W.; Schenning, A. P. H. J. About Supramolecular Assemblies of π-Conjugated Systems. *Chem. Rev.* **2005**, *105* (4), 1491–1546.
(97) Socrates, G. *Infrared and Raman Characteristic Group Frequencies: Tables and Charts*; John Wiley & Sons, 2004.
(98) Hunter, C. A. Quantifying Intermolecular Interactions: Guidelines for the Molecular Recognition Toolbox. *Angew. Chem. Int. Ed Engl.* **2004**, *43* (40), 5310–5324.
(99) Buaksuntear, K.; Limarun, P.; Suethao, S.; Smitthipong, W. Non-Covalent Interaction on the Self-Healing of Mechanical Properties in Supramolecular Polymers. *Int. J. Mol. Sci.* **2022**, *23* (13). https://doi.org/10.3390/ijms23136902.
(100) van Duffel, B.; Verbiest, T.; Van Elshocht, S.; Persoons, A.; De Schryver, F. C.; Schoonheydt, R. A. Fuzzy Assembly and Second Harmonic Generation of Clay/Polymer/Dye Monolayer Films. *Langmuir* **2001**, *17* (4), 1243–1249.
(101) Zhu, T.; Jiang, Z.; Ma, Y. Adsorption of Nanoparticles and Nanoparticle Aggregates on Membrane under Gravity. *Appl. Phys. Lett.* **2013**, *102* (15), 153109.
(102) Thor, K. Calcium—Nutrient and Messenger. *Front. Plant Sci.* **2019**, *10*. https://doi.org/10.3389/fpls.2019.00440.
(103) White, P. J.; Broadley, M. R. Calcium in Plants. *Ann. Bot.* **2003**, *92* (4), 487–511.
(104) Eklund, L.; Eliasson, L. Effects of Calcium Ion Concentration on Cel Wall Synthesis. *J. Exp. Bot.* **1990**, *41* (7), 863–867.
(105) Ortenzi, M. A.; Antenucci, S.; Marzorati, S.; Panzella, L.; Molino, S.; Rufián-Henares, J. Á.; Napolitano, A.; Verotta, L. Pectin-Based Formulations for Controlled Release of an Ellagic Acid Salt with High Solubility Profile in Physiological Media. *Molecules* **2021**, *26* (2). https://doi.org/10.3390/molecules26020433.
(106) Lara-Espinoza, C.; Carvajal-Millán, E.; Balandrán-Quintana, R.; López-Franco, Y.; Rascón-Chu, A. Pectin and Pectin-Based Composite Materials: Beyond Food Texture. *Molecules* **2018**, *23* (4). https://doi.org/10.3390/molecules23040942.
(107) Weiss, M.; Fan, J.; Claudel, M.; Sonntag, T.; Didier, P.; Ronzani, C.; Lebeau, L.; Pons, F. Density of Surface Charge Is a More Predictive Factor of the Toxicity of Cationic Carbon Nanoparticles than Zeta Potential. *J. Nanobiotechnology* **2021**, *19* (1), 5.
(108) Kah, M.; Kookana, R. S.; Gogos, A.; Bucheli, T. D. A Critical Evaluation of Nanopesticides and Nanofertilizers against Their Conventional Analogues. *Nat. Nanotechnol.* **2018**, *13* (8), 677–684.
(109) Sharma, V.; Tiwari, P.; Mobin, S. M. Sustainable Carbon-Dots: Recent Advances in Green Carbon Dots for Sensing and Bioimaging. *J. Mater. Chem. B Mater. Biol. Med.* **2017**, *5* (45), 8904–8924.
(110) Borgatta, J. R.; Lochbaum, C. A.; Elmer, W. H.; White, J. C.; Pedersen, J. A.; Hamers, R. J. Biomolecular Corona Formation on CuO Nanoparticles in Plant Xylem Fluid. *Environ. Sci.: Nano* **2021**, *8* (4), 1067–1080.
(111) Xing, B.; Mason, S. E.; Hamers, R. J.; White, J. C. Advanced Material Modulation of Nutritional and Phytohormone Status Alleviates Damage from Soybean Sudden Death Syndrome. *Nanotechnology* **2020**.

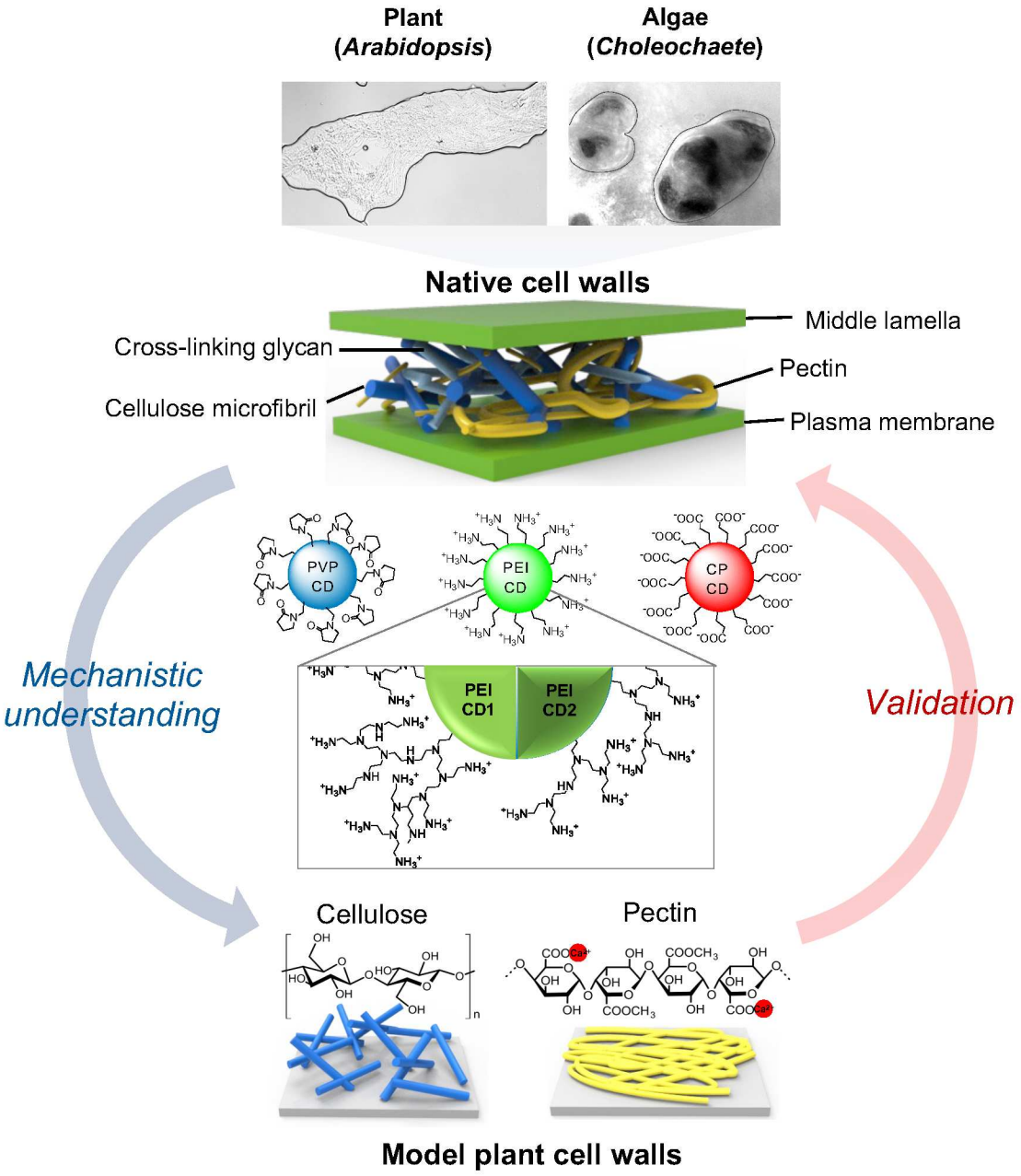

Figure 1. Interactions of nanoparticles with model cell walls and native cell walls of plants and algae. Novel model planar surfaces made of cellulose or pectin were developed for understanding their interactions with carbon dots (CD) that were designed by of positive, neutral and negative charge. Confocal microscopy, FTIR, XPS, and QCM-D analysis were performed with model cell walls interfaced with CD. The underlying mechanisms of CD-cell wall interactions were validated using native cell walls isolated from *Arabidopsis* plants and green algae (*Coleochaete spp.*) cell walls *in vivo*.

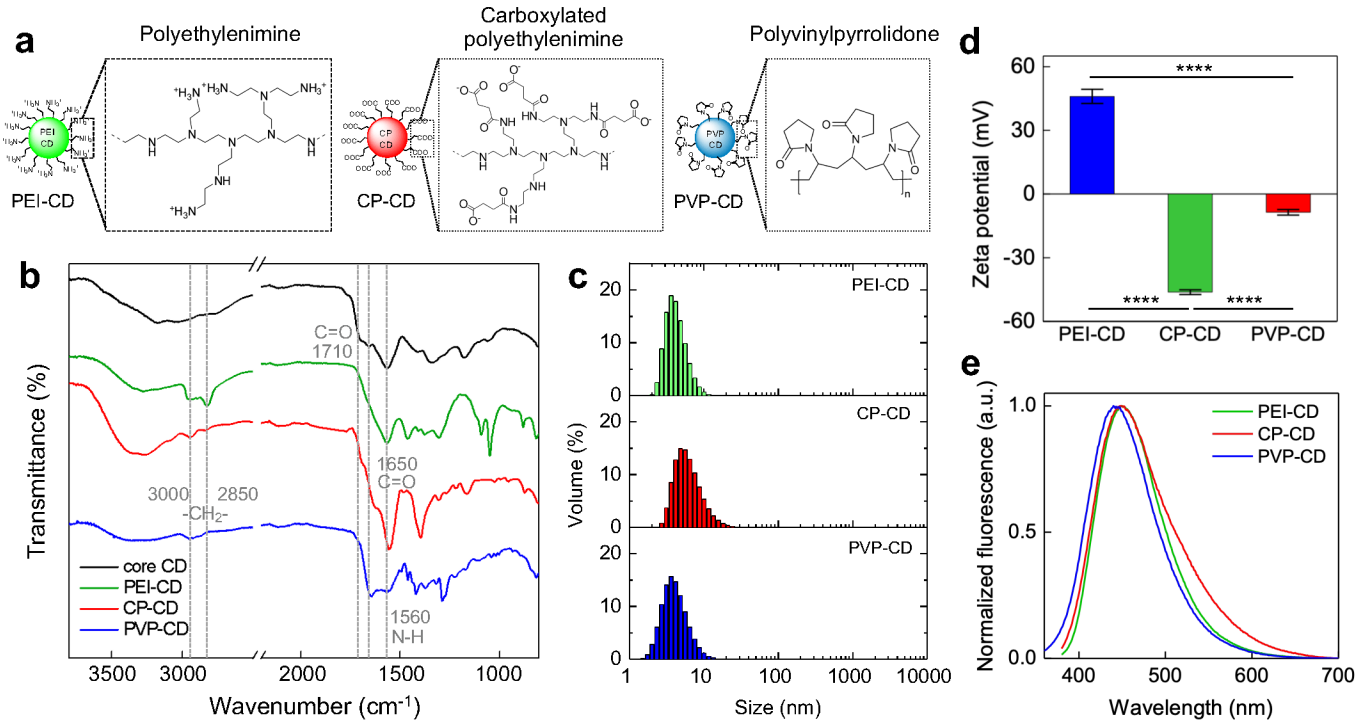

Figure 2. Characterization of carbon dots (CD). a) CD were functionalized with PEI, CP, and PVP for synthesizing nanoparticles with different surface charges. **b)** The FTIR spectra indicated characteristic bands for the three types of CD. **c)** The CD exhibit similar hydrodynamic diameter and **d)** contrasting positive, neutral and negative zeta potentials (mean ± standard deviation, *n*=5). Means were compared by one-way ANOVA followed by post hoc comparison using the Tukey test. **** $p < 0.0001$. **e)** CD have similar fluorescence emission upon 355 nm excitation.

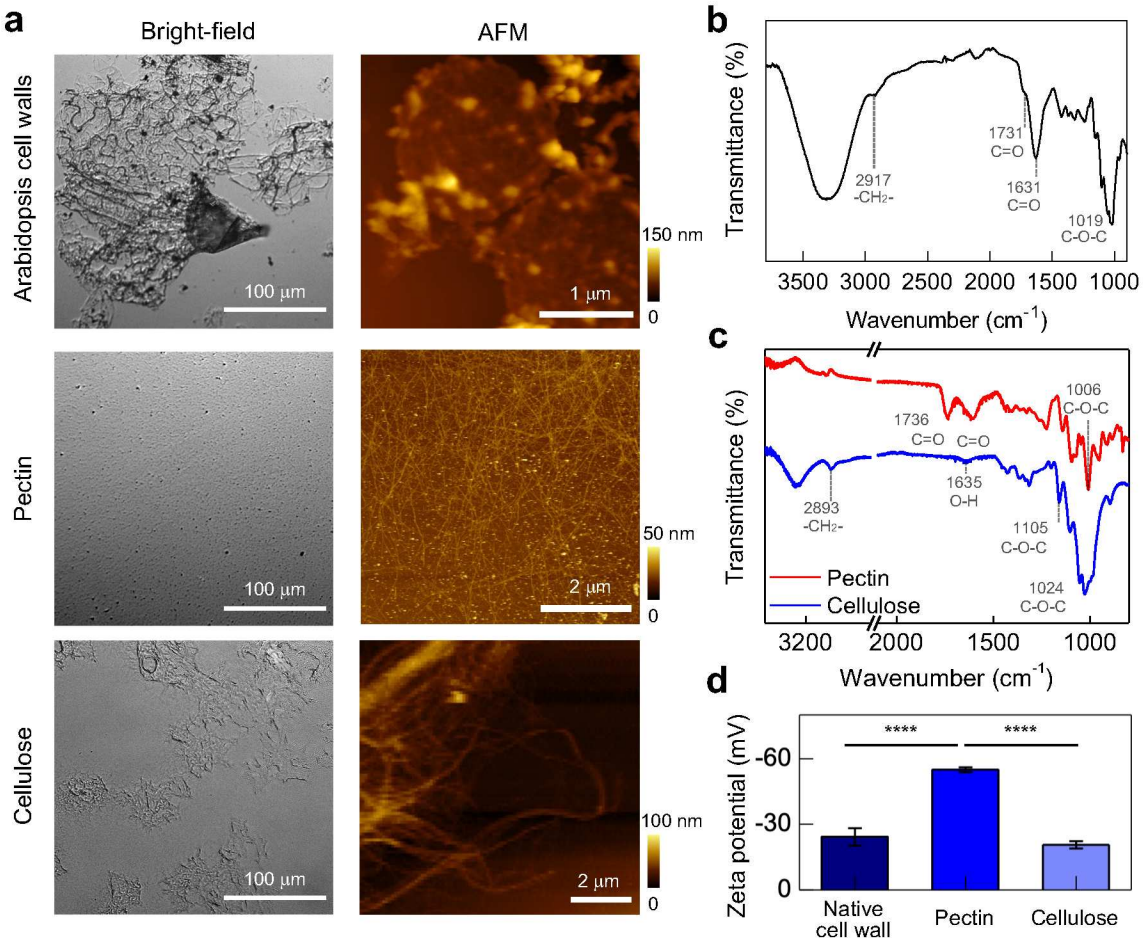

Figure 3. Model and native cell wall component characterization. a) Bright-field microscopy image and AFM image of native cell wall extracted from Arabidopsis leaf, pectin, and cellulose model cell wall surfaces. Scale bar for a bright-field image: 100 µm. FT-IR spectra of **b)** native plant cell wall **c)** pectin and cellulose model cell wall surfaces. **d)** Zeta potentials of native and model cell walls (10 mM TES buffer, 0.1 mM NaCl, pH 7.4) (one-way ANOVA, Tukey test, n=5). **** $p<0.0001$

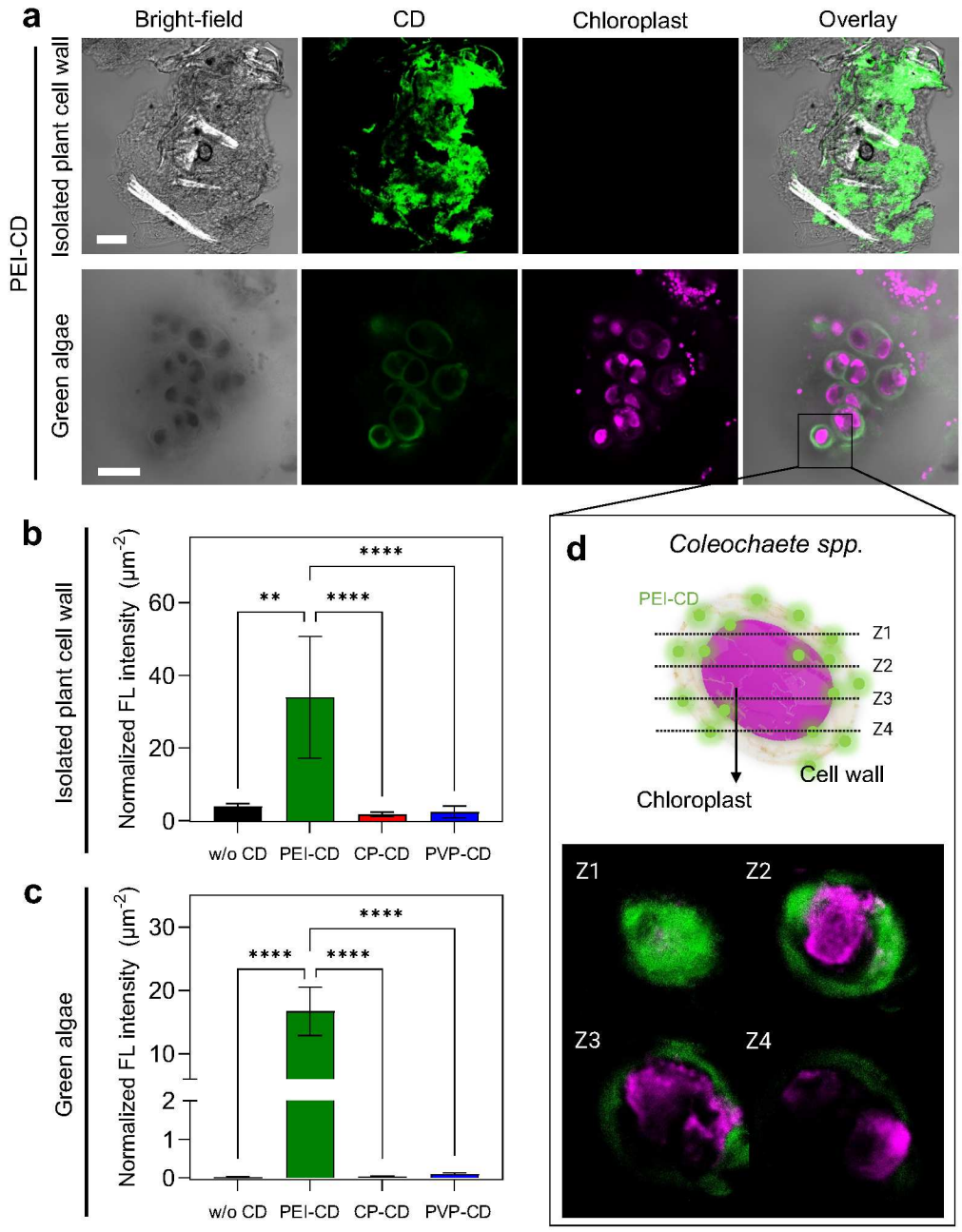

Figure 4. Interactions of carbon dots with native plant and algae cell walls. a) Representative confocal images of native cell walls isolated from *Arabidopsis* plant leaves and from live green algae (*Coleochaete*) that were exposed to PEI-CD. The native cell walls displayed a fluorescence emission characteristic of CD, indicating a binding affinity with positively charged PEI-CD. Scale bar, 100 µm. **b-c)** Comparative analysis of CD fluorescence intensity normalized by imaging area of native plant and algae cell walls from multiple confocal images (n = 3-9). Different letters represent significant differences, (one-way ANOVA, Tukey test), ** p< 0.01, **** p<0.0001. **d)** z-stack images displaying the PEI-CDs bound to algae cell wall and membrane and surrounding chloroplasts (magenta).

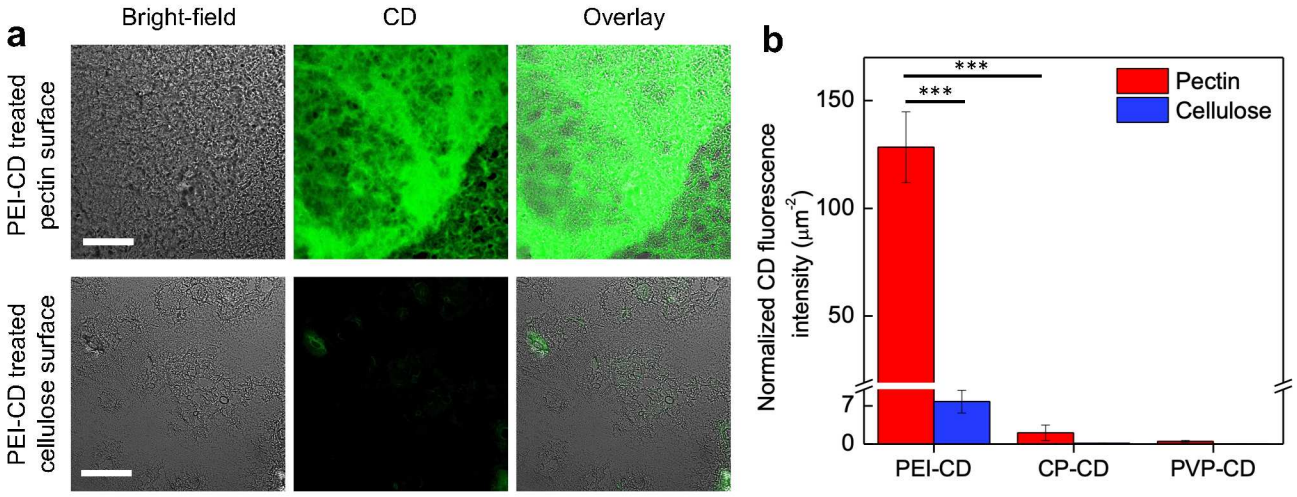

Figure 5. Model cell wall interactions with carbon dots. a) Representative confocal images of pectin and cellulose surfaces exposed to PEI-CDs indicate a stronger affinity of these positively charged CD with pectin than cellulose. Scale bar, 100 μm. **b)** Comparison of the integrated CD fluorescence intensity per area of pectin and cellulose surfaces. One-way ANOVA, Tukey test, n=3-4, *** $p < 0.001$.

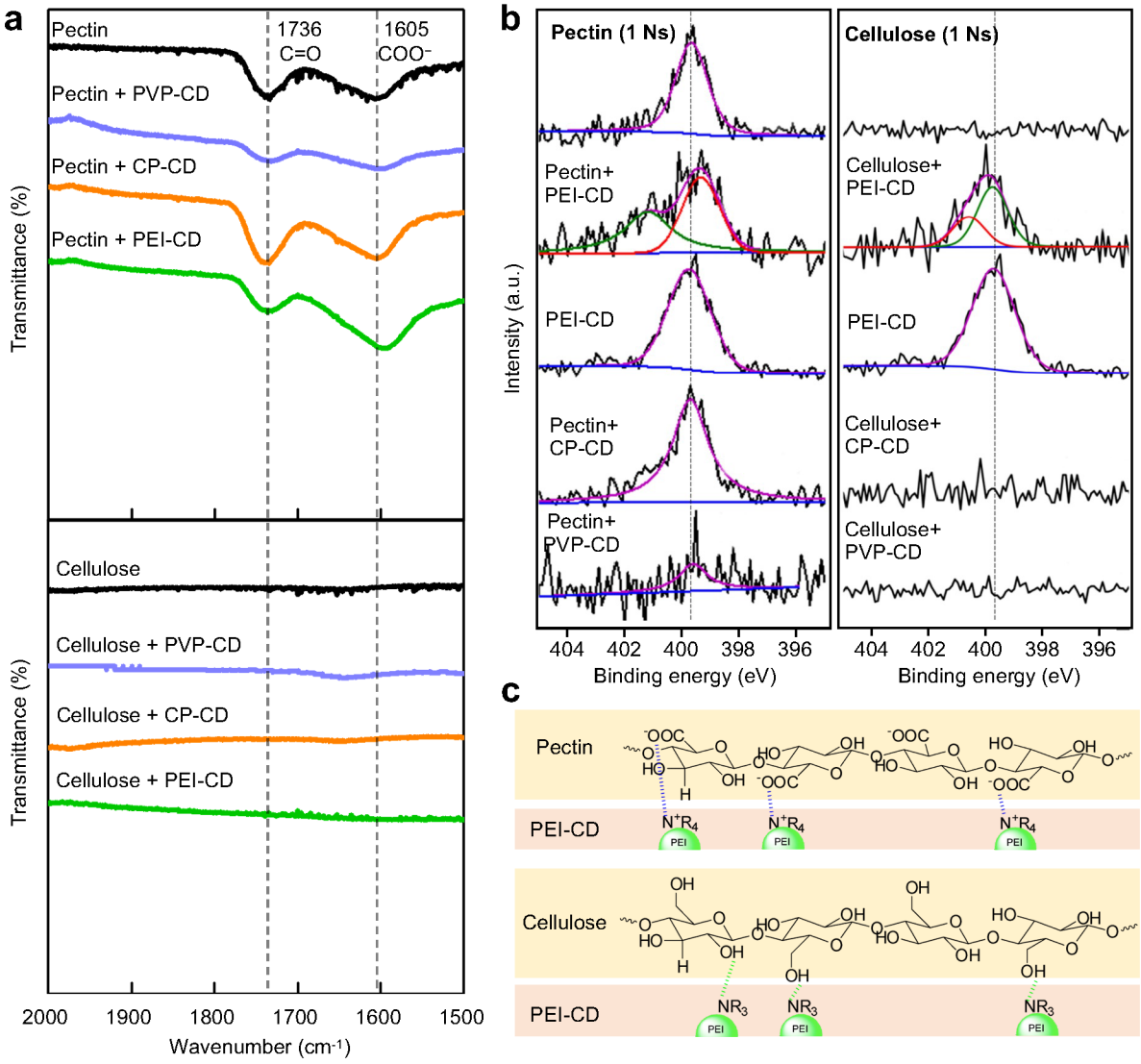

Figure 6. Chemical interactions between plant cell wall model surfaces and carbon dots. a) FTIR spectra of pectin and cellulose model surfaces interfaced with CD (PEI-CD, CP-CD, and PVP-CD) and without nanoparticles (control). Pectin but not cellulose model cell walls interfaced with PEI-CD shows both a peak shift and intensity enhancement in the frequency range (1500 to 2000 cm^{-1}) where CD have characteristic vibration bands. **b)** XPS spectra of pectin and cellulose model surfaces with and without CD (PEI-CD, CP-CD, and PVP-CD) treatment. A new XPS peak emerged for PEI-CD treated pectin model surfaces at 401.3 eV corresponding to the N 1s in quaternary ammonium cations that can be attributed to the proton transfer from carboxyl groups in pectin to amine groups on PEI-CD. A blue shifted N 1s peak was observed for PEI-CD treated cellulose model surfaces from 399.6 to 400.1 eV, that can be explained by the formation of hydrogen bonds between PEI-CD amine and amide groups and cellulose hydroxyl groups. **c)** Schematic illustrating the molecular level interactions between pectin and cellulose model cell wall surfaces and PEI-CD.

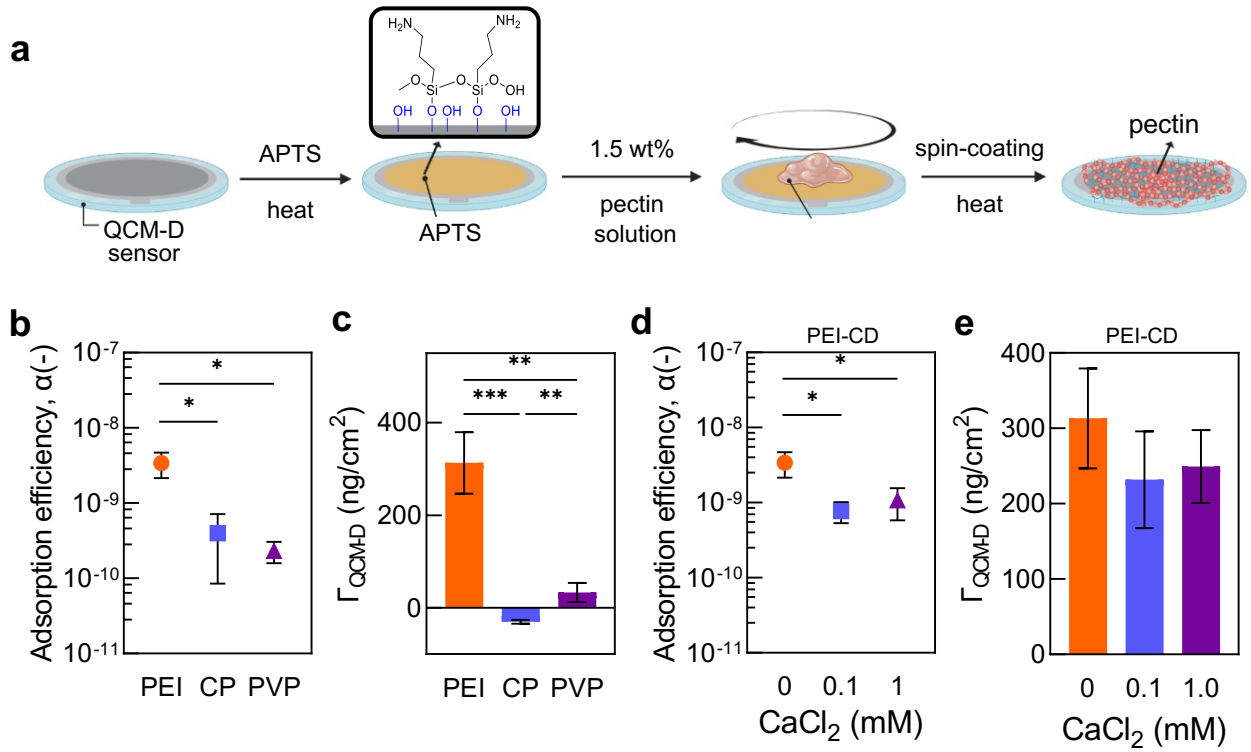

Figure 7. **Real-time interactions of carbon dots with pectin model cell wall surfaces. a)** Schematic figure of SiO_2 QCM-D sensor spin coating with pectin. PEI-, CP-, and PVP- CD **b)** adsorption efficiency and **c)** acoustic mass density after rinse. Effect of Ca^{2+} on PEI-CD **d)** adsorption efficiency, and **e)** acoustic mass density after rinse in pectin model surface (0 – 1 mM $CaCl_2$) ($p>0.05$). Error bars indicate standard deviations (n=3). One-way ANOVA, Tukey test. * $p<0.05$; ** $p<0.01$; *** $p<0.001$.

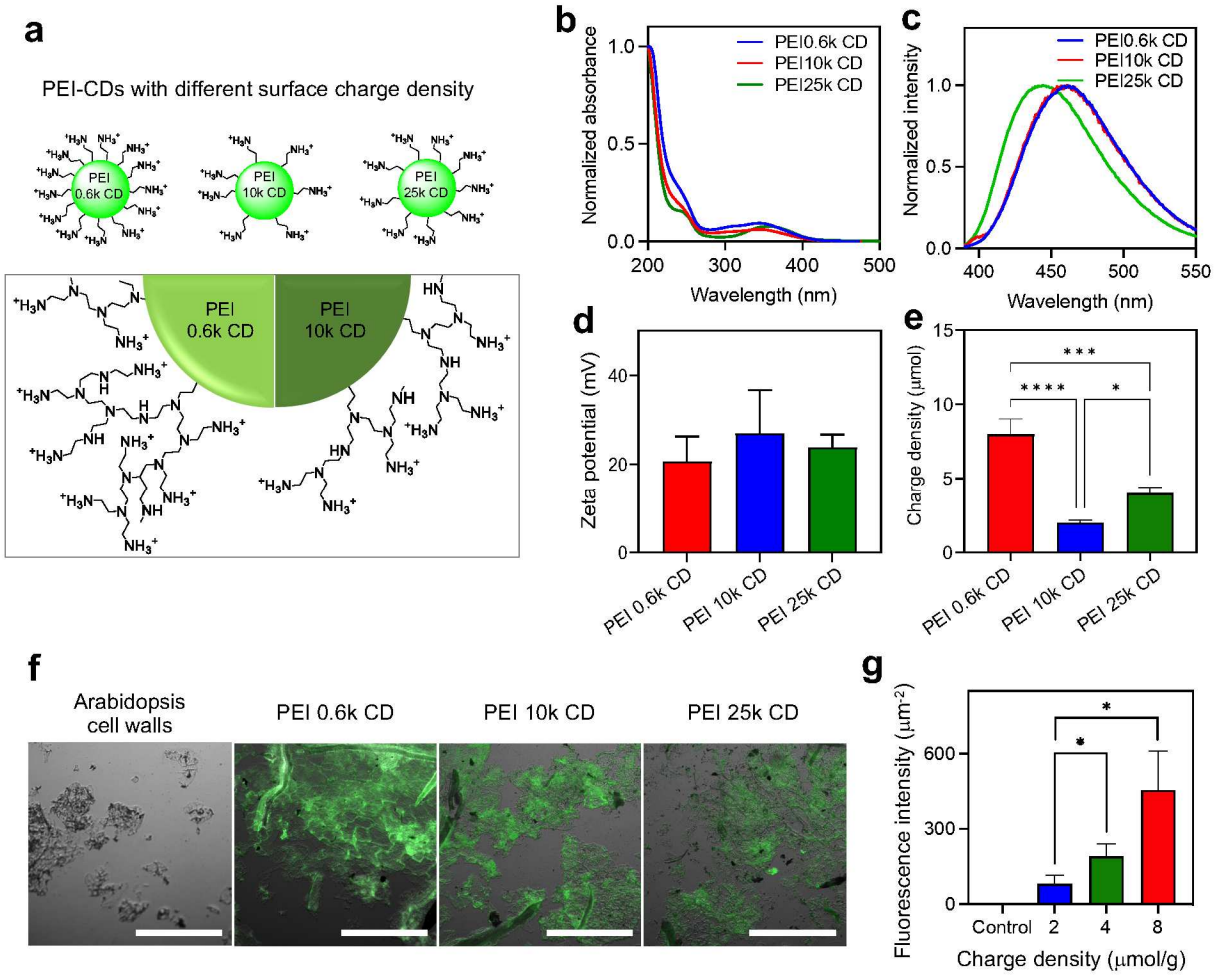

Figure 8. Effect of surface charge density of positively charged carbon dots on their interactions with plant cell walls. a) Positively charged CDs were functionalized using PEI polymers with different molecular weights (0.6k, 10k, and 25k) to modify their surface charge density. **b-c)** Absorption and fluorescence spectra of PEI-CDs , and **d)** zeta potentials were similar for PEI 0.6k, 10k, and 25k CDs (10 mM TES buffer, pH 7) ($p>0.05$). **e)** The surface charge density of PEI-CDs was determined by polyelectrolyte titration. (One-way ANOVA, post hoc. n=3, *, $p<0.05$; ***, $p<0.001$; ****, $p<0.0001$). **f)** Representative confocal images of pectin surfaces exposed to PEI-CDs and **g)** integrated PEI-CD fluorescence intensity per area analysis, indicate a stronger affinity of high surface charged density PEI-CD 0.6k to pectin. Scale bar, 100 μm. One-way ANOVA, Tukey test, n=3-4, * $p< 0.05$, *** $p< 0.001$, **** $p< 0.0001$.

Table of Content